

High Efficiency Desulfurization of Synthesis Gas

Annual Report

September 2000 – August 2001

Anirban Mukherjee
Kwang-Bok Yi
Elizabeth J. Podlaha
Douglas P. Harrison

November 2001

DE-PS26-00FT40813

Gordon A. and Mary Cain Department of Chemical Engineering
Louisiana State University
Baton Rouge, LA 70803

DISCLAIMER

This report was prepared as an account of work sponsored by an agency of the United States Government. Neither the United States Government nor any agency thereof, nor any of their employees, makes any warranty, express or implied, or assumes any legal liability or responsibility for the accuracy, completeness, or usefulness of any information, apparatus, product, or process disclosed, or represents that its use would not infringe privately owned rights. Reference herein to any specific commercial product, process, or service by trade name, trademark, manufacturer, or otherwise does not necessarily constitute or imply its endorsement, recommendation, or favoring by the United States Government or any agency thereof. The views and opinions of authors expressed herein do not necessarily state or reflect those of the United States Government or any agency thereof.

ABSTRACT

Mixed metal oxides containing CeO_2 and ZrO_2 are being studied as high temperature desulfurization sorbents capable of achieving the DOE Vision 21 target of 1 ppmv of less H_2S . The research is justified by recent results in this laboratory that showed that reduced CeO_2 , designated CeO_n ($1.5 < n < 2.0$), is capable of achieving the 1 ppmv target in highly reducing gas atmospheres. The addition of ZrO_2 has improved the performance of oxidation catalysts and three-way automotive catalysts containing CeO_2 , and should have similar beneficial effects on CeO_2 desulfurization sorbents.

An electrochemical method for synthesizing CeO_2 - ZrO_2 has been developed and the products have been characterized by XRD and TEM during year 01. Nanocrystalline particles having a diameter of about 5 nm and containing from approximately 10 mol% to 80 mol% ZrO_2 have been prepared. XRD showed the product to be a solid solution at low ZrO_2 contents with a separate ZrO_2 phase emerging at higher ZrO_2 levels. Phase separation did not occur when the solid solutions were heat treated at 700°C .

A flow reactor system constructed of quartz and teflon has been constructed, and a gas chromatograph equipped with a pulsed flame photometric detector (PFPD) suitable for measuring sub-ppmv levels of H_2S has been purchased with LSU matching funds. Preliminary desulfurization tests using commercial CeO_2 and CeO_2 - ZrO_2 in highly reducing gas compositions has confirmed that CeO_2 - ZrO_2 is more effective than CeO_2 in removing H_2S . At 700°C the product H_2S concentration using CeO_2 - ZrO_2 sorbent was near the 0.1 ppmv PFPD detection limit during the prebreakthrough period.

TABLE OF CONTENTS

Disclaimer	<i>i</i>
Abstract	<i>ii</i>
Table of Contents	<i>iii</i>
List of Figures	<i>iv</i>
List of Tables	<i>v</i>
Executive Summary	<i>vi</i>
1. Introduction	1
1.1. High Temperature Gas Desulfurization	1
1.2. Ceria-Zirconia Catalyst Research	3
2. Electrochemical Synthesis and Characterization of $\text{Ce}_{1-x}\text{Zr}_x\text{O}_2$	4
2.1 Electrochemical Experimental	4
2.2 Solid State Analyses	5
2.3 Electrosynthesis Results and Discussion	6
2.3.1 Compositional	6
2.3.2 XRD and TEM Characterization	7
2.3.3 Electrochemical Process Characterization	12
3. High Temperature Desulfurization	16
3.1. Fixed-Bed Reactor	16
3.2. Gas Analysis	18
3.3. Materials	20
3.4. Preliminary Results	23
4. Conclusions	26
5. References	27

LIST OF FIGURES

Figure 1.	Electrochemical Cell Schematic	5
Figure 2.	Electrolyte Concentration vs. Final Powder Composition	6
Figure 3.	TEM Images of (a) Ceria, (b) Ceria-7 at.% Zirconia and (c) Ceria-18 at.% Zirconia	8
Figure 4.	Selected-Area Electron Diffraction (SAED) Pattern	
Figure 5.	XRD Analysis of (a) the Electrochemically Generated Nanocrystalline $Ce_{0.82}Zr_{0.18}O_2$, (b) Cubic CeO_2 (JCPDS 34-394), and (c) Monoclinic (JCPDS 37-1484) and Tetragonal (JCPDS 42-1164) ZrO_2 Peaks.	10
Figure 6.	XRD Patterns for Three Different $Ce_{1-x}Zr_xO_2$ Samples, Where x Represents the Mol Fraction of Zirconia.	11
Figure 7.	A Comparison Between the LSU and Commercial NexTech XRD Powder Pattern.	11
Figure 8.	Heat Treated 700 °C, 18.7 mol % Zr Ceria-Zirconia With Resulting Crystallite Size of (a) 9.5 nm, (b) 10 nm, (c) 11 nm, (d)12 nm, (e) 12.5 nm, (f), 12.5 nm, and (g)14.5 nm. Heat Treated Times Shown at Left.	12
Figure 9.	TEM Micrograph of 18.7 at. % Zr After 106 hrs of Heat Treatment at 700 °C.	13
Figure 10.	Heat Treated 700 °C, 65.2 mol % Zr Ceria-Zirconia With Resulting Crystallite Size of (a) 4 nm, (b) 5 nm, (c) 6 nm, (d,e) 7 nm and (g) 8 nm. Heat Treated Times Shown at Left.	13
Figure 11.	TEM Micrograph of 65.2 at. % Zr After 106 hr of Heat Treatment at 700 °C.	14
Figure 12.	Current Characteristics for the Ce and Ce-Zr Electrolyte at an Applied Potential of -2.0 V and Stagnant Solution.	15
Figure 13.	Current Characteristics of Ceria-Zirconia in Quiescent Solution C and With a Stirring Speed of 900 rpm, Both With an Applied Potential of -2.0 V.	15
Figure 14.	Polarization Curves Corrected for Ohmic Drop, Solution C for a Scan Rate of 5 mv/s.	16
Figure 15.	Fixed-Bed Reactor System.	17
Figure 16.	Details of the Quartz Reactor.	18
Figure 17.	Chromatograph Sampling Arrangement	21
Figure 18.	PFPD Calibration Curve.	22
Figure 19.	PFPD Chromatogram Corresponding to 0.01 ppmv H_2S	22
Figure 20.	TCD Calibration Curve.	23
Figure 21.	Typical Breakthrough Curve Showing H_2S Concentration in the Reactor Product as a Function of Time.	24
Figure 22.	The Effect of Pre-reduction on H_2S Concentration Using CeO_2 Sorbent.	25
Figure 23.	Comparison of H_2S Concentrations Using CeO_2-ZrO_2 and CeO_2	26

LIST OF TABLES

Table 1. Composition of the Various Electrolyte Solutions.	5
Table 2. Resistivity of Solution C at Various Times of Deposition.	16
Table 3. Gas Chromatograph Operating Conditions.	19
Table 4. Selected Properties of CeO ₂ and CeO ₂ -ZrO ₂ Used in Preliminary Fixed-Bed Reactor Tests.	20

EXECUTIVE SUMMARY

The recently released DOE Vision 21 program requires much more stringent control of H₂S concentration in coal-derived synthesis gas. Previous target levels of about 20 ppmv H₂S suitable for electric power generation using an integrated gasification combined cycle process (IGCC) have been replaced by H₂S targets of 1 ppmv or less required for fuel cell and other catalytic processes.

Zinc-based sorbents developed for IGCC applications are not capable of achieving the Vision 21 target at high temperatures. Reduced cerium oxide, CeO_n (1.5 < n < 2.0) has recently been shown to be capable of reducing H₂S to less than 1 ppmv at temperatures near 700°C, but only in gas atmospheres having considerable greater reducing power than typical coal-derived gases. Related research in oxidation catalysis and three-way automotive catalysis has shown that performance has been improved by the addition of ZrO₂ to the CeO₂. The reasons given for the improved performance, including increased oxygen exchange capacity, should also result in improved desulfurization performance.

This research project consists of two major activities – the electrochemical synthesis and characterization of CeO₂-ZrO₂ materials, and high temperature desulfurization tests using CeO₂-ZrO₂ sorbents.

Nanocrystalline powders of approximately 5 nm grain diameter and containing from 10 mol% to 80 mol% ZrO₂ have been deposited at an electrode surface using the cathodic generation of base method. Conditions required for the production of desired solid solutions of CeO₂-ZrO₂ having a fluorite-type of structure have been identified. A separate ZrO₂ phase is formed as the concentration of ZrO₂ is increased. Heat treatment at 700°C for as long as 106 hrs at 700°C produced no phase separation, but the crystallite size increased from 5 nm to 14.5 nm.

A laboratory-scale fixed-bed reactor having a capacity of about 15 g of solid has been constructed for desulfurization testing. In order to avoid interaction between low concentrations of H₂S and stainless steel, all components of the reactor and analytical systems that may be exposed to low H₂S concentrations are constructed of quartz, teflon, or silcosteel. Reactor product gas composition as a function time is determined using a Varian 3800 gas chromatograph purchased for this project with LSU matching funds. The chromatograph is equipped with a pulsed flame photometric detector (PFPD) for measuring low H₂S concentrations (< ≈ 10 ppmv) and a thermal conductivity detector (TCD) for higher concentrations of H₂S.

A limited number of preliminary desulfurization tests using pure CeO₂ from Rhone Poulenc and a commercial CeO₂-ZrO₂ material from NexTech containing 80 mol% CeO₂ have been completed. Tests using pure CeO₂ have confirmed earlier results showing more efficient H₂S removal was possible using a sorbent pre-reduced in a sulfur-free atmosphere than when the reduction and desulfurization steps occurred simultaneously. In addition, at equivalent reaction conditions, pre-reduced CeO₂-ZrO₂

was more effective in removing H₂S than pre-reduced CeO₂ alone. In desulfurization tests at 700°C and 1 atm in a feed gas containing 1.25 mol % H₂S, 50 mol% H₂, balance N₂, the prebreakthrough H₂S concentration using pre-reduced CeO₂-ZrO₂ was near the PFPD calibration limit of 0.1 ppmv compared to prebreakthrough H₂S concentration of 0.3 ppmv using pure CeO₂.

I. INTRODUCTION

Research relating to the high temperature desulfurization of coal-derived gas has been a major component of the DOE fossil energy program for a number of years. In the past, the primary objective was to reduce H₂S concentration to levels required for electric power generation using integrated gasification combined cycles (IGCC), approximately 20 ppmv. Desulfurization processes for this application using zinc-based sorbents have progressed to the demonstration stage. The new DOE Vision 21 program, however, requires much more stringent sulfur control measures. Sulfur levels equal to or less than 1ppmv are required for fuel cells and certain synthesis gas catalytic processes. New sorbents are needed to meet these more stringent sulfur limits.

Recent research in this laboratory (Zeng et al. 1999, Zeng et al., 2000) showed that reduced cerium oxide, designated CeO_n (1.5 < n < 2.0), is capable of reducing H₂S from 1 mol% to less than 1ppmv at temperatures near 700°C in highly reducing gas compositions. However, the product compositions from gasifiers currently available in the United States (Texaco, KRW, etc.) do not have the reducing power required to achieve significant CeO₂ reduction. The equilibrium H₂S content in contact with unreduced CeO₂ is well above the more stringent Vision 21 target levels.

The current research is investigating the desulfurization performance of mixed oxide sorbents of CeO₂-ZrO₂ with the objective of meeting Vision 21 target levels in less reducing gas compositions. The addition of ZrO₂ to CeO₂ has improved the performance of oxidation catalysts and three-way automotive catalysts. The improvement is attributed to increased reducibility and improved oxygen mobility resulting from the addition of ZrO₂, factors that should also improve desulfurization performance.

1.1. High Temperature Gas Desulfurization

High temperature desulfurization of coal-derived gas is based on the noncatalytic gas-solid reaction between H₂S and an appropriate metal oxide. The reaction may be written generically as follows



The generic reaction for the regeneration of the metal sulfide is

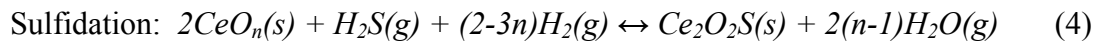
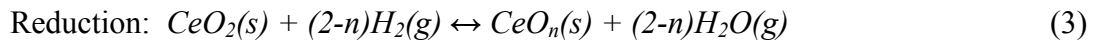


For economic reasons, the sorbent must maintain activity through many sulfidation-regeneration cycles. A number of metals including Zn, Fe, Mn, Cu, and Ca have been studied but most of the recent research has focused on Zn-based materials, including ZnO (e.g., Gibson and Harrison 1980), ZnFe₂O₄ (e.g., Focht et al. 1988), and xZnO•TiO₂ (e.g., Woods et al. 1990).

Harrison (1998) has discussed the advantages and disadvantages of zinc-based sorbents. Advantages include favorable desulfurization thermodynamics, rapid kinetics, large stoichiometric sulfur capacity (39 g S/100 g ZnO), and relatively low cost. Disadvantages include the tendency for ZnO to be reduced to volatile metallic Zn at high temperature, the highly exothermic nature of the regeneration reaction, and the possible formation of ZnSO₄ during regeneration. The tendency for ZnO reduction followed by Zn vaporization can be moderated, but not eliminated, by the addition of TiO₂ to form the mixed metal oxide xZnO•TiO₂. However, TiO₂ addition increases the sorbent processing cost and reduces the sulfur capacity. Dilute O₂ is used to control temperature during regeneration, but this causes dilute SO₂ to be produced and complicates the ultimate sulfur control problem. ZnSO₄, because of its large molar volume, has been identified as a cause of rapid sorbent deterioration in multicycle tests, and careful control of temperature and the partial pressures of O₂ and SO₂ are required to prevent its formation.

The performance of CeO₂ as a high temperature desulfurization sorbent was recently studied in this laboratory (Zeng et al. 1999, Zeng et al., 2000). H₂S concentrations were reduced from 1 mol% (10,000 ppmv) to 1 ppmv or less at temperatures in the range of 650°C to 800°C in highly reducing atmospheres. Reduction of CeO₂ to oxygen-deficient CeO_n (n < 2) was the key in achieving low H₂S concentrations. The sulfided product, Ce₂O₂S, was easily regenerated using SO₂ with sulfur liberated in elemental form. Preliminary multicycle tests (25 complete cycles) showed no evidence of sorbent deterioration.

The complete cycle using cerium sorbent consists of three steps – reduction, sulfidation, and regeneration – as shown by the following reactions.



The ultimate degree of reduction, i.e., the equilibrium value of n, depends on temperature and the oxygen partial pressure of the reducing gas, as described by Bevan and Kordis (1964) and Sorensen (1976). Electrobalance experiments in this laboratory have shown that level of reduction, i.e., the experimental value of n, is in close agreement with the results of Bevan and Kordis. Unfortunately the oxygen partial pressure in the product gas from Texaco and KRW gasifiers is too large to achieve significant CeO₂ reduction.

The current research is examining the addition of ZrO₂ to CeO₂ in the hope that reduction to CeO_n can be more easily accomplished. The expected benefits are based on results from recent research in the areas of oxidation and automotive catalysis summarized in the following section.

1.2. Ceria-Zirconia Catalyst Research

CeO₂ serves an important role in three-way automotive catalysts (TWC) by regulating the gas phase oxygen pressure. During fuel rich operation, CeO₂ is reduced to CeO_n and the oxygen released assists in the oxidation of CO and hydrocarbons to CO₂. Under fuel lean conditions CeO_n is oxidized to CeO₂ and removal of oxygen from the gas phase assists in the reduction of NO_x to N₂. In oxidation catalysis, the CeO₂ is reduced to CeO_n by surface adsorbed species as they are oxidized to CO₂, and the CeO_n is then re-oxidized to CeO₂ by oxygen from the gas phase.

Recent research as shown that the addition of ZrO₂ to CeO₂ enhances the redox reactions. Colon et al. (1998) state that the addition of ZrO₂ enhances the oxygen mobility within the crystal and improves the catalyst thermal stability at 1000°C. Zamar et al. (1995) discuss the enhanced oxygen storage and release capacity of CeO₂-ZrO₂ mixtures used for CH₄ combustion. ZrO₂ was said to promote the formation of oxygen vacancies and increase the mobility of bulk oxygen. The 50% CH₄ conversion level was reached at a temperature 130°C lower using Ce_{0.8}Zr_{0.2}O₂ compared to CeO₂ alone.

Hori et al. (1998) report an increase in reversibly stored oxygen by a factor of 1.7-2.5 for phase separated CeO₂-ZrO₂ compared to CeO₂ alone, and by a factor of 3-5 for solid solutions of CeO₂-ZrO₂. The optimum Zr concentration was 25 mol%, but performance was relatively insensitive to Zr loading between 15 mol% and 50 mol%. Bunlesin et al. (1997) found that addition of ZrO₂ slowed the deactivation rate for CO oxidation over a Ce-Pd catalyst. Deactivation without ZrO₂ was attributed to a large increase in crystallite size, and ZrO₂ was said to slow crystallite growth.

Trovarelli et al. (1997) and Cuif et al. (1996) discuss the improved performance of three-way automotive catalysts due to the addition of ZrO₂ to CeO₂. Trovarelli et al. state that the addition of ZrO₂ enhances the catalytic, textural, redox, and oxygen storage properties of ceria. Trovarelli (1996) and Ozawa (1997) have published recent reviews describing the beneficial effects of ZrO₂ addition.

These positive effects on the performance of CeO₂ catalysts associated with ZrO₂ addition – improved redox potential, increased oxygen mobility, higher oxygen exchange capacity, improved activity at lower temperature, and increased thermal stability – are the same factors needed to improve the performance of ceria-based desulfurization sorbents, and the objective of the current research is to demonstrate that ceria-zirconia sorbents are capable of achieving Vision 21 desulfurization goals in typical coal gas compositions.

The project is divided into two major activities – the electrochemical synthesis and characterization of CeO₂-ZrO₂ mixtures and the high temperature desulfurization using CeO₂-ZrO₂ sorbents. While both activities have been addressed during year 01, synthesis and characterization have been emphasized. Year 01 accomplishments on both activities are described in the following.

2. ELECTROCHEMICAL SYNTHESIS AND CHARACTERIZATION OF $Ce_{1-x}Zr_xO_2$

A number of methods have been used for producing ceria-zirconia mixtures, including bulk co-precipitation, rapid solidification, high-energy mechanical milling, laser evaporation-condensation and sol-gel. An alternative electrochemical route was recently demonstrated by Switzer (1987) and Yanchun et al. (1995) for ceria and zirconia, respectively, but not the mixture $Ce_{1-x}Zr_xO_2$. Independently, the powders were deposited by the cathodic generation of base method at an electrode surface. In our work, we have altered the synthesis method in order to codeposit the powders and to investigate the chemical composition, phase structure and crystallite size as a function of the processing parameters. The effect of heat treatment on the resulting crystalline structure was also noted. Conditions have been identified for producing ceria-zirconia mixtures that exhibit solid solutions of the fluorite-type structure, are nanocrystalline, and have about 25 mol % zirconia, which are recommended as the first choice for future desulfurization testing.

2.1. Electrochemical Experimental

Figure 1 shows the two-compartment electrochemical cell employed in the powder synthesis under potentiostatic control. The anolyte and catholyte are separated by a glass frit. A platinum mesh was used as the anode. The reference electrode was a saturated calomel electrode (SCE). An inverted, stationary, stainless steel shaft-disk electrode was used as described by Podlaha *et al.* (1997) with the electrode surface facing upwards in an electrolyte to avoid blockage of the electrode surface by trapped H_2 gas bubbles, produced from water and proton reduction. The stainless steel disc electrodes (AISI 304L) were embedded inside an epoxy resin such that only one side of the metal disc was exposed to the electrolyte. A thin, stainless steel shaft, encased in Teflon was screwed into the disc-epoxy assembly. The shaft was threaded allowing electrical contact to the disc. The depositions were carried out under unstirred conditions without rotating the electrode, and stirred electrolyte conditions with the electrode rotated.

The electrolyte consisted of 0.5 M ammonium nitrate, and varying concentrations of zirconyl (IV) nitrate hydrate and cerium (III) nitrate hexahydrate. All experiments were carried at room temperature of 23 ± 1 °C. Table 1 lists the different compositions of the electrolyte used. The pH was maintained at 1.5 ± 0.1 at the start of each experiment.

Potentiostatic experiments were carried out with a BAS-Zahner IM6(e) system. Three different potentials of -1.8 V, -1.9 V and -2.0 V vs SCE were applied to investigate the effect of potential on the deposition. DC current was used in all the experiments conducted. Polarization curves were measured with BAS-Zahner IM6(e) potentiostat/galvanostat by ramping the potential at sweep rates of 5, 10, 25, 50, 100, 200, 500, 750 and 1000 mV/s. The deposited powders were scraped from the electrode, dried

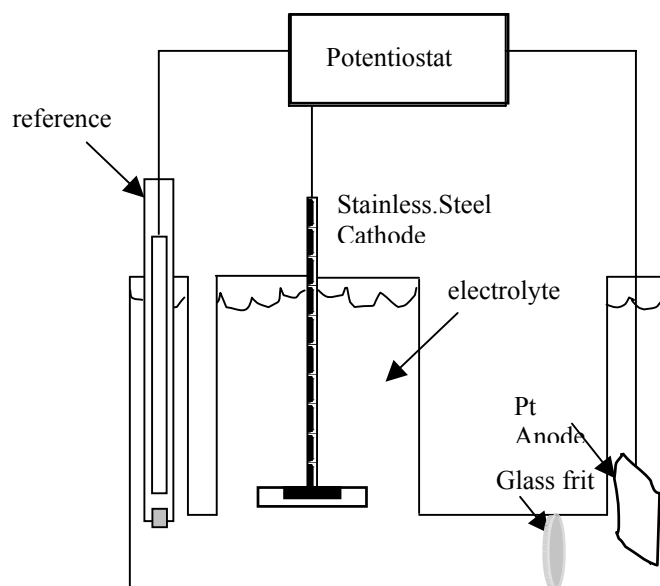


Figure 1. Electrochemical Cell Schematic

Table 1. Composition of the Various Electrolyte Solutions.

Electrolyte	Ce(NO ₃) ₃ .6H ₂ O	Zr(NO ₃) ₄ .H ₂ O	NH ₄ NO ₃ (M)
A	0.5	0.0	0.5
B	0.5	0.1	0.5
C	0.5	0.2	0.5
D	0.25	0.2	0.5
E	0.125	0.2	0.5
F	0.25	0.5	0.5
G	0.125	0.5	0.5

in a dessicator at room temperature and analyzed. The ohmic drop was measured with a BAS-Zahner IM6(e) Impedance Analyzer.

2.2. Solid State Analyses

The chemical composition of the deposit was measured by energy dispersive x-ray fluorescence spectroscopy (EDXRF), (Kevex, Model Omicron) calibrated with bulk samples of ceria and zirconia. The composition was determined over a large region of pressed sorbent powder to verify uniformity of the ceria-zirconia mixture. The spot size of the x-ray analysis is a projection from a 100 micron collimeter and the chemical composition was mapped over an area of several centimeters. Four to five measurements

were averaged for each sample of powder with a Rh tube potential of 45 kV, current of 0.8 mA (shaping index of 64) in an air atmosphere, using 400 seconds sampling time. Once the powder concentration was found in the desired range of 15-50 mol % zirconia, further analysis by x-ray diffraction (XRD) and transmission electron microscopy (TEM) were carried out to verify the structure of the material. The crystallinity and particle size of the as produced powder was analyzed by a bright-field high resolution TEM (JEOL Model JEM 2010). Specimens for the TEM were made by dispersing the powders in a solution of 10 % methanol in water. A drop of the suspension was put on a holey carbon film and allowed to dry for analysis. The TEM analysis of the nanocrystalline $Ce_{1-x}Zr_xO_2$ were done at 200 keV with a point to point resolution of 23 nm. The phase identification of the sample and the lattice parameters were determined with x-ray diffraction analysis (XRD), carried out using a Bruker Advance D8 powder diffractometer equipped with a focusing Ge (111) incident beam monochromator ($Cu-K_{\alpha 1}$ radiation). Finely ground samples were placed on a zero-background quartz sample holder. Intensity data were collected at ambient temperature in the 2θ range between 25° and 60° with a step width of 0.02° and a 8 s count time. The peaks of each compound were compared with phases in the International Center for Diffraction Data database (ICDD).

2.3. Electrosynthesis Results and Discussion

2.3.1. Composition

Figure 2 shows the parametric representation of final powder composition vis-à-vis the initial electrolyte concentration at various applied potentials. A linear relationship is

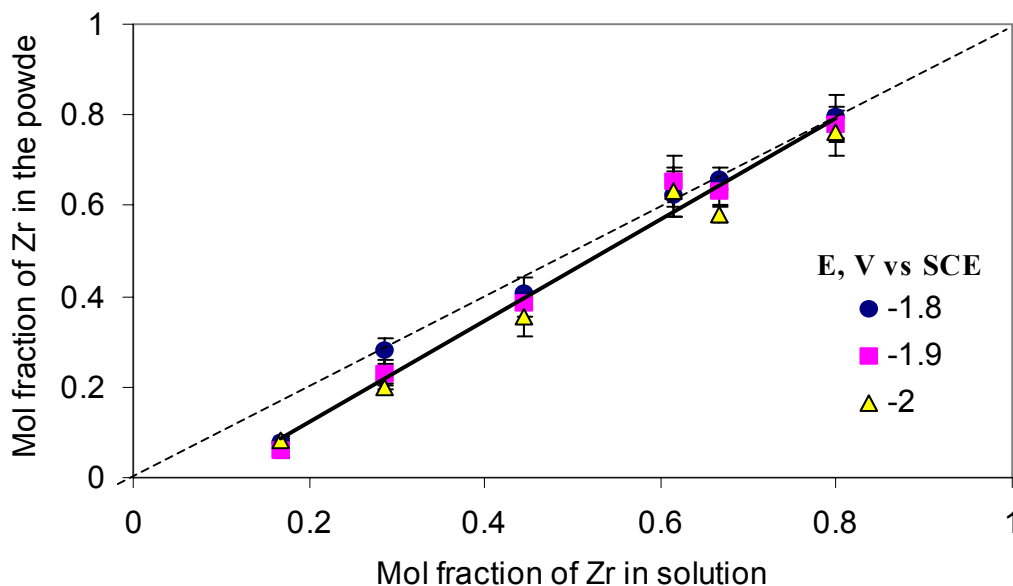


Figure 2. Electrolyte Concentration vs. Final Powder Composition.

observed between the concentration of Zr in the powder with the concentration in the electrolyte. The aim was to obtain a composition between 15 to 50 mol % of Zr in the final powder for optimal catalytic conditions, and was achieved by controlling the electrolyte concentrations. Additionally, the powder composition was not found to be a function of the applied potential. At low Zr concentrations in the electrolyte ceria is preferentially deposited over zirconia, which diminishes as the concentration of Zr in the solution increases. As a reference point, a dashed line has been added to Figure X2 to show the 1:1 correspondence between the mol fraction of Zr in the powder with concentration in solution.

2.3.2. XRD and TEM Characterization

The microstructure of the $\text{Ce}_{1-x}\text{Zr}_x\text{O}_2$ with $x = 0, 0.07, 0.18$ mol Zr fraction sample was characterized by TEM. Figure 3 shows high-resolution TEM images of the sample. The average grain size of the nanocrystallites were approximately 5 nm in diameter, independent of composition. Crystallite size of this order competes with many of the standard wet and dry processing production methods.

The structure of the nanocrystallites was examined by electron diffraction. Figure 4 shows a selected-area electron diffraction (SAED) pattern taken from Figure 3 (c) for the 18 at. % Zr case. The discrete rings indicate a crystalline material and is consistent with the lattice fringes observed in Figures 3 (a)-(c). The first 7 diffraction rings (start from the center) correspond to the (1 1 1), (2 0 0), (2 2 0), (3 1 1), (2 2 2), (4 0 0) and (3 3 1) reflections of the CeO_2 , and suggest a solid solution.

The crystallite size and phase can also be verified with X-ray diffraction (XRD). The XRD of the powder sample having 18 at % Zr, produced from solution C, is shown in Figure 5 (a). It is compared to the standard libraries of the end members (b) cubic Ce and (c) monoclinic and tetragonal Zr. Neither monoclinic nor tetragonal modification of ZrO_2 was observed in the x-ray powder diffraction pattern of the sample. The spectrum exhibits a cubic single phase similar to other solid solution $\text{ZrO}_2\text{-CeO}_2$ XRD patterns of samples generated by non-electrochemical techniques. The mean crystal size, calculated from the full width at half maximum of the (111) reflection, was 4.5 nm, which is consistent with the TEM observation.

As the concentration of Zr is increased in the powder an emergence of a 2nd phase is seen (Figure 6). The slight shift to the right of the main (111) peak indicates a decrease of the lattice parameter due to Zr incorporation. The shift provides evidence of the formation of a solid solution, that has been associated with superior catalytic properties Colon et al. (1998). Formation of a separate ZrO_2 phase is undesirable from a catalytic perspective.

Comparing the LSU electrosynthesized 18 % at. Zr powder with a commercial ceria-zirconia solid solution reveals a similar XRD pattern. Figure 7 shows that the (111) peak is slightly broader than a commercial product by NexTexch due to the smaller grain

size. A small shift of the peaks from the commercial product to the right indicate a higher Zr concentration than the LSU synthesized one in the solid solution.

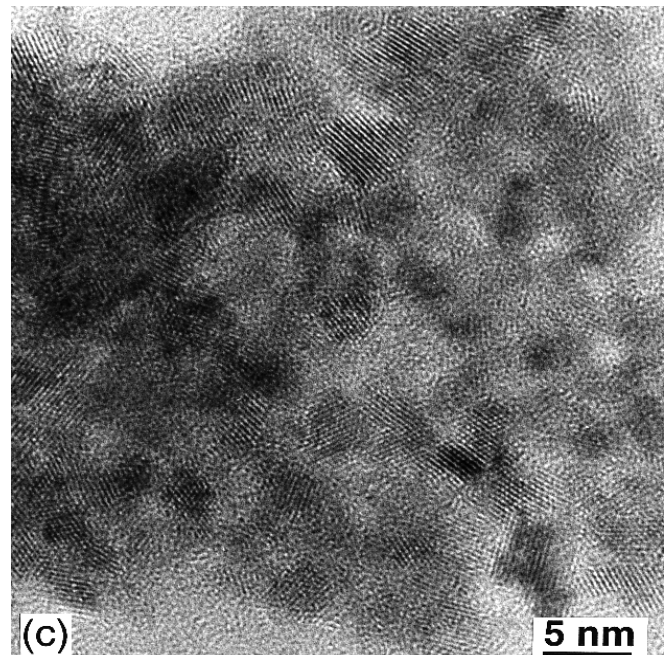
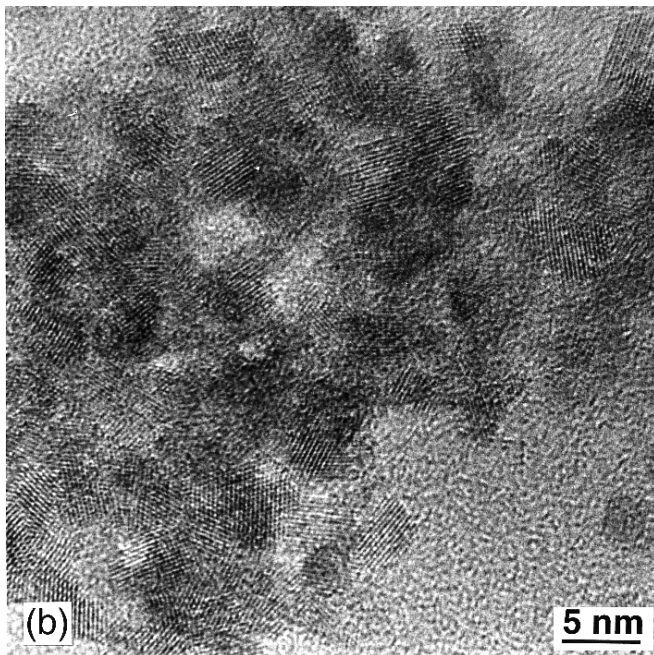
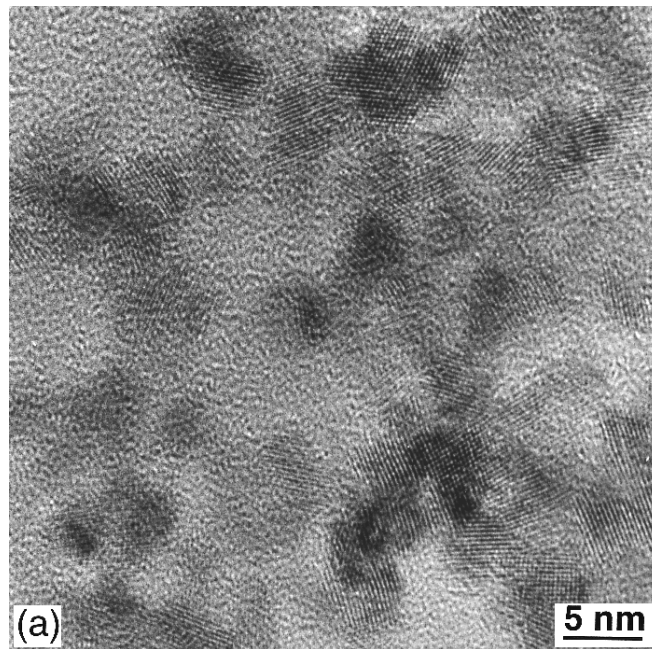


Figure 3. TEM images of (a) Ceria, (b) Ceria-7 at.% Zirconia and (c) Ceria-18 at.% Zirconia

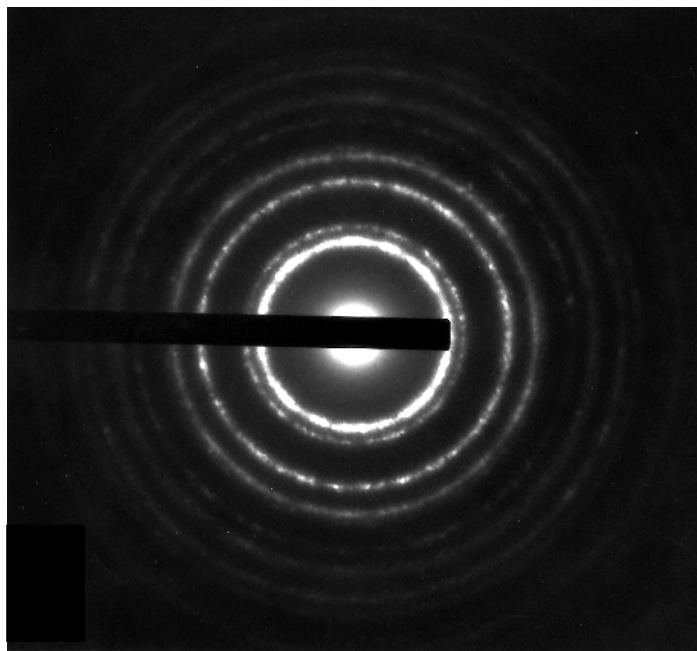


Figure 4. Selected-Area Electron Diffraction (SAED) Pattern Taken Over a Large Area Shown in Figure 3.

Nanostructured crystallite size and the presence of a solid solution are prerequisites for a quality sorbent material, in addition to its stability at high temperature. Since the reactor will be operated at temperatures $> 600\text{ }^{\circ}\text{C}$ the affect of a heat treatment was considered. XRD and TEM analysis are shown in Figures 8-11. The XRD pattern of a heat treated sample at $700\text{ }^{\circ}\text{C}$ from solution C is shown in Figure 8, having a Zr composition of 18.7 mol %. The choice of temperature was determined from desulfurization results using ceria sorbents (Zeng et al. 1999 and Zeng et al. 2000). A heat treatment was carried out for 2 hr on a single sample, which was then cooled to room temperature to conduct the XRD analysis. The sample was then subjected to another heat treatment along with a cooling cycle for XRD testing. The procedure was repeated with the following heating times: 2, 2, 3, 5, 10, 24, 60 hr. Figure 8 shows the characteristic ceria peaks at heat heating step corresponding to a solid solution as well as Al, which was present in the holder and not part of the powder. Additionally, phase separation was not observed upon heat treatment.

The particle size was found to increase slightly at different heat treatment steps, but after 106 hours of heating at 700°C , the crystallite size was 14.5 nm. Large increases in crystallite size is not considered desirable, but the increase observed here is small enough that it is not considered critical for the catalytic sorbent property. Figure 9 is a TEM micrograph that verifies the increase in crystallite size observed with XRD. The micrograph was taken after cooling of the last heat treatment at 106 hrs. Lattice fringes are present as previously observed.

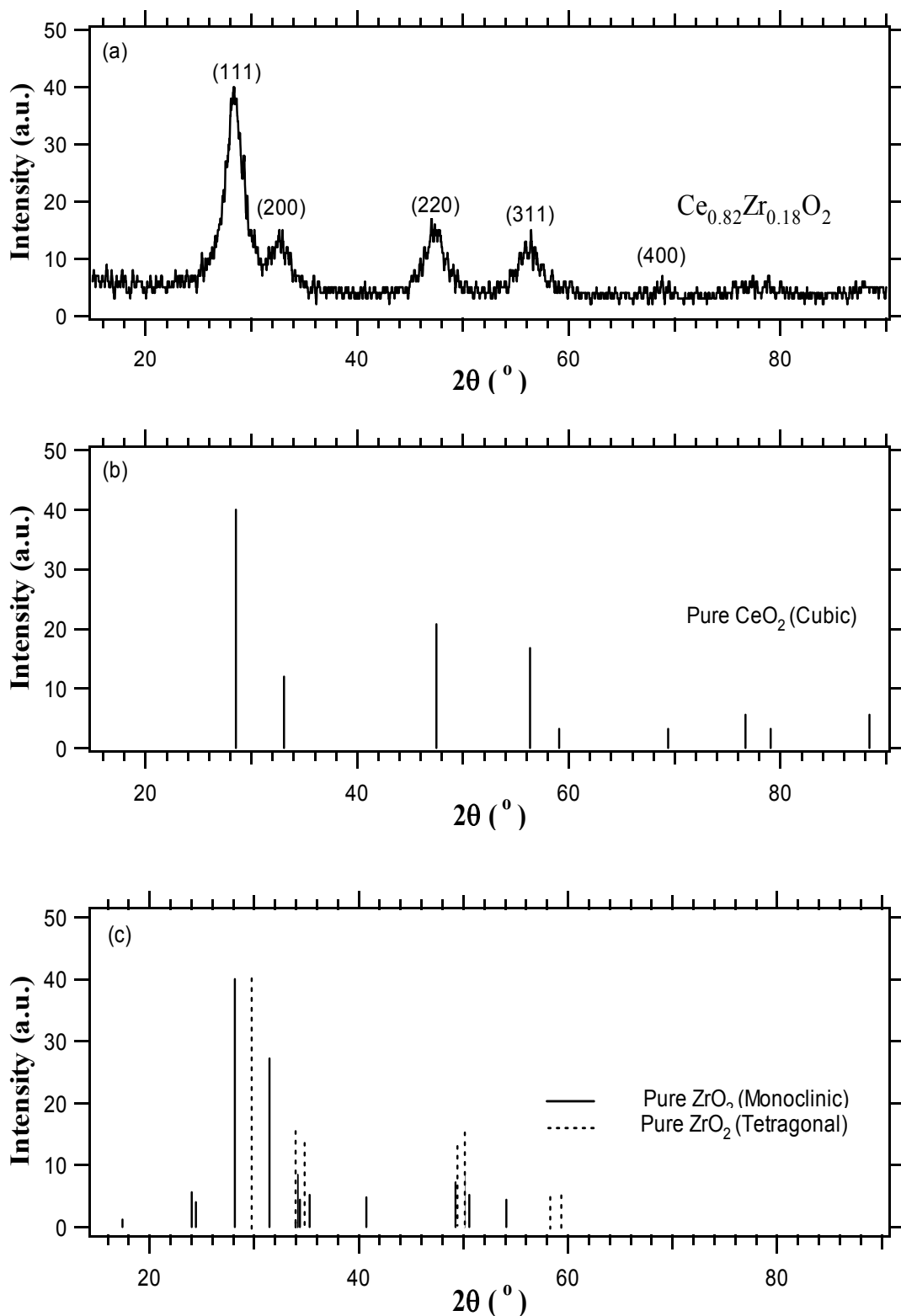


Figure 5. XRD Analysis of (a) the Electrochemically Generated Nanocrystalline $\text{Ce}_{0.82}\text{Zr}_{0.18}\text{O}_2$, (b) Cubic CeO_2 (JCPDS 34-394), and (c) Monoclinic (JCPDS 37-1484) and Tetragonal (JCPDS 42-1164) ZrO_2 Peak

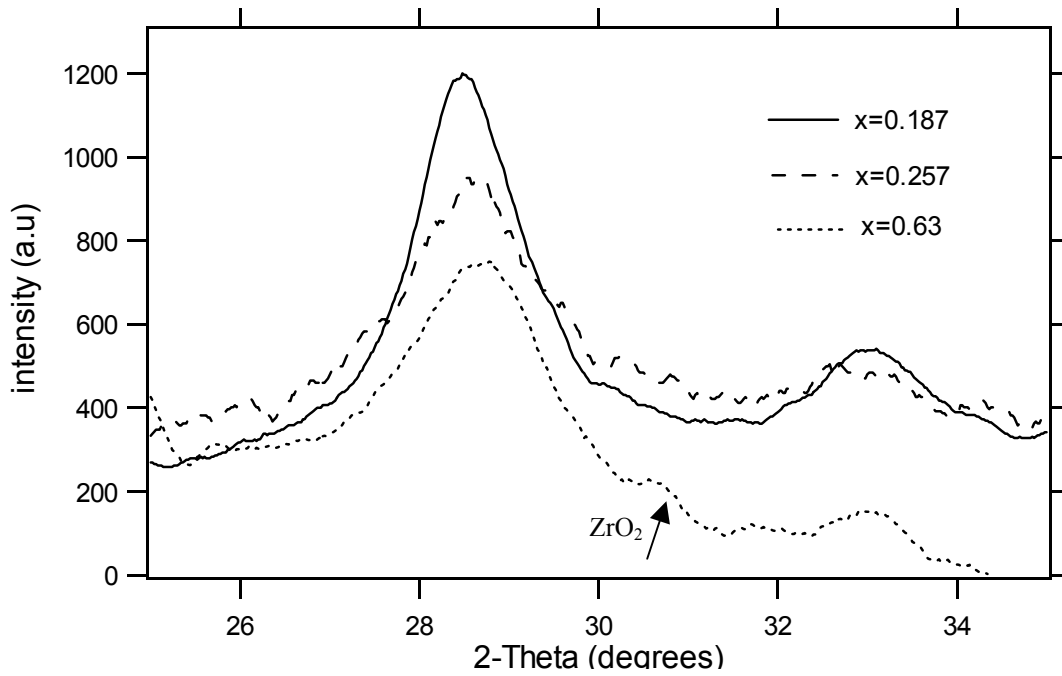


Figure 6. XRD Patterns for Three Different $\text{Ce}_{1-x}\text{Zr}_x\text{O}_2$ Samples, Where x Represents the Mol Fraction of Zirconia.

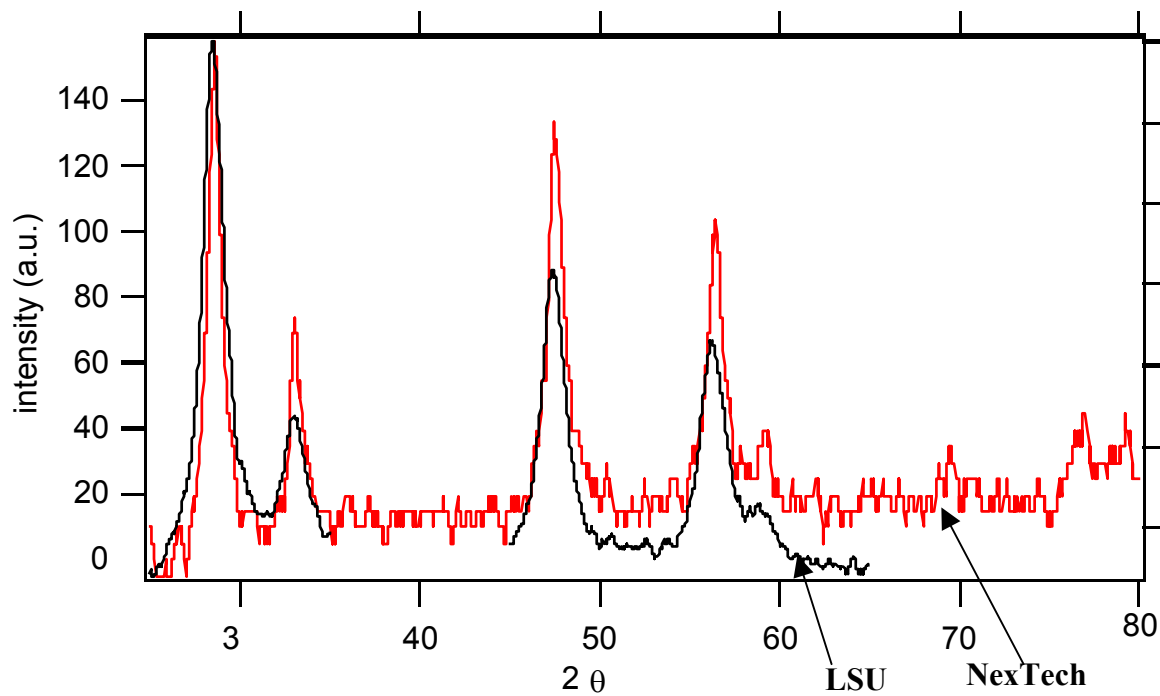


Figure 7. A Comparison Between the LSU and Commercial NexTech XRD Powder Pattern.

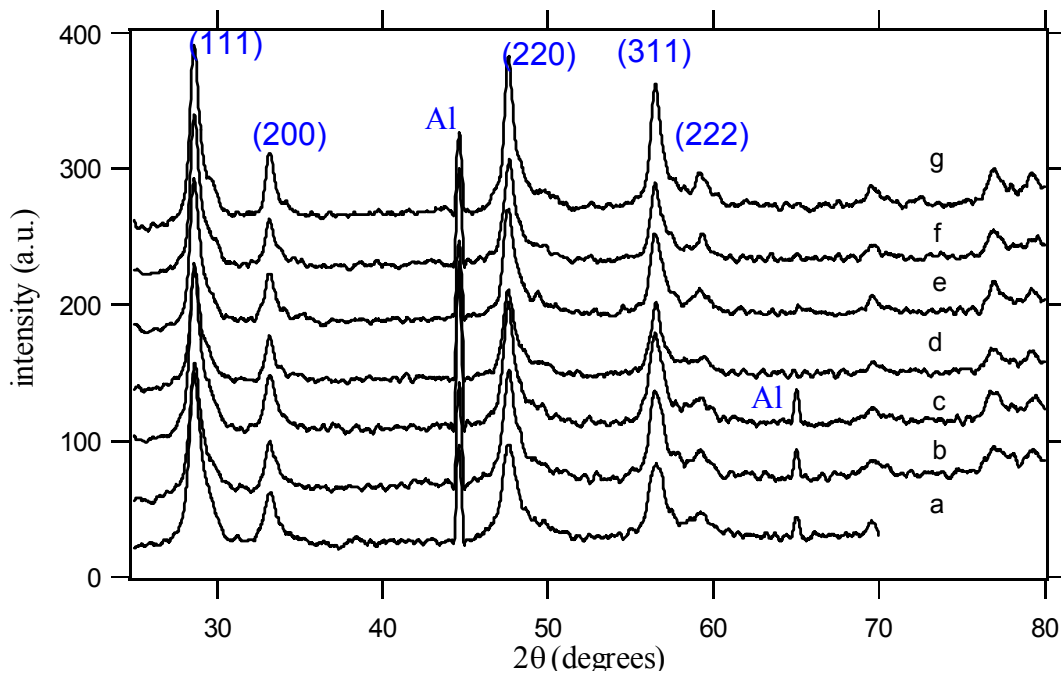


Figure 8. Heat Treated 700 °C, 18.7 mol % Zr Ceria-Zirconia with Resulting Crystallite Size of (a) 9.5 nm, (b) 10 nm, (c) 11 nm, (d)12 nm, (e) 12.5 nm, (f), 12.5 nm, and (g)14.5 nm. Heat Treated Times Shown at Left.

Figure 10 is a heat treatment carried out on a sample which exhibits two distinct phases, one a mixture of ceria-zirconia and another pure zirconia, indicated by the vertical lines. Heat treatment was carried out at 700 °C and the procedure was the same as for the low Zr sample. Upon heat treatment there is no evidence of phase changes. Also, the crystallite size increases with heat treatment with a terminal size of 10 nm after 106 hr of heating. Similarly to Figure 9, Figure 11 confirms the crystallite size with TEM.

2.3.3 Electrochemical Process Characterization

Figure 12 shows the current characteristics of pure ceria and a ceria-zirconia mixture (18 mol% of zirconia). As expected the current decreases with time as more and more of the electrode surface becomes covered by powder. The initial curve is steeper for pure ceria suggesting that the rate of powder deposition is faster for pure ceria compared to the ceria-zirconia powder.

Figure 13 compares the current characteristics for quiescent and "stirred" solutions. Electrolyte stirring was induced by the rotation of the electrode. The current density for the stirred case was larger in magnitude and had more fluctuations than the unstirred experiment. The current fluctuations were likely due to the fact that the powder

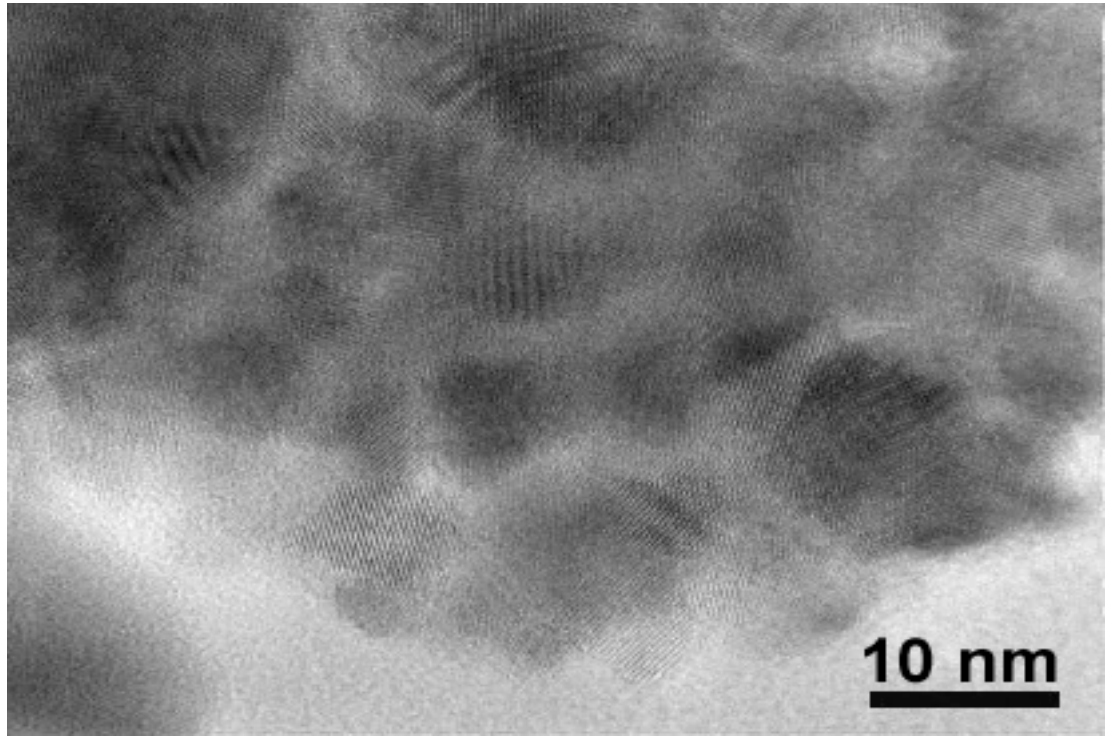


Figure 9. TEM Micrograph of 18.7 at. % Zr After 106 hrs of Heat Treatment at 700 °C

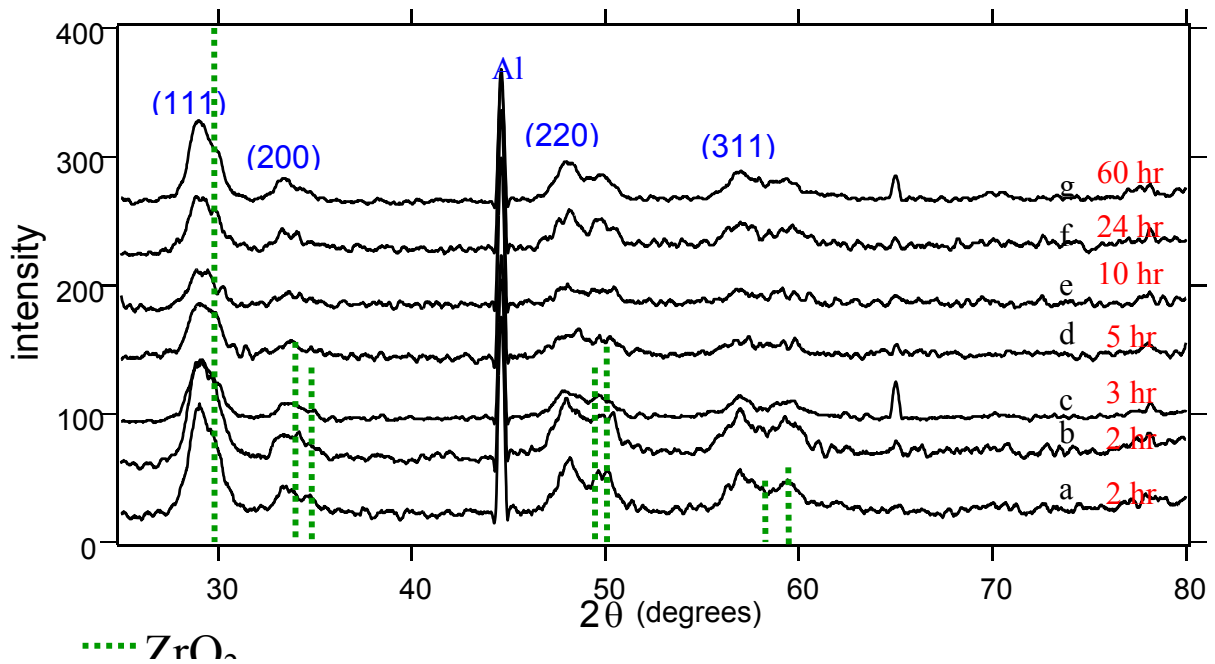


Figure 10. Heat Treated 700 °C, 65.2 mol % Zr Ceria-Zirconia With Resulting Crystallite Size of (a) 4 nm, (b) 5 nm, (c) 6 nm, (d,e) 7 nm and (g) 8 nm. Heat Treated Times Shown at Right

became dislodged from the surface while stirring, thereby creating new exposed areas on the electrode surface. The quantity of powder obtained with stirring was less than that for the unstirred case. The rate of deposition was 16 mg/min without stirring and 6 mg/min with stirring. The overall increase in the current density with stirring identifies a transport controlled electrochemical reactant.

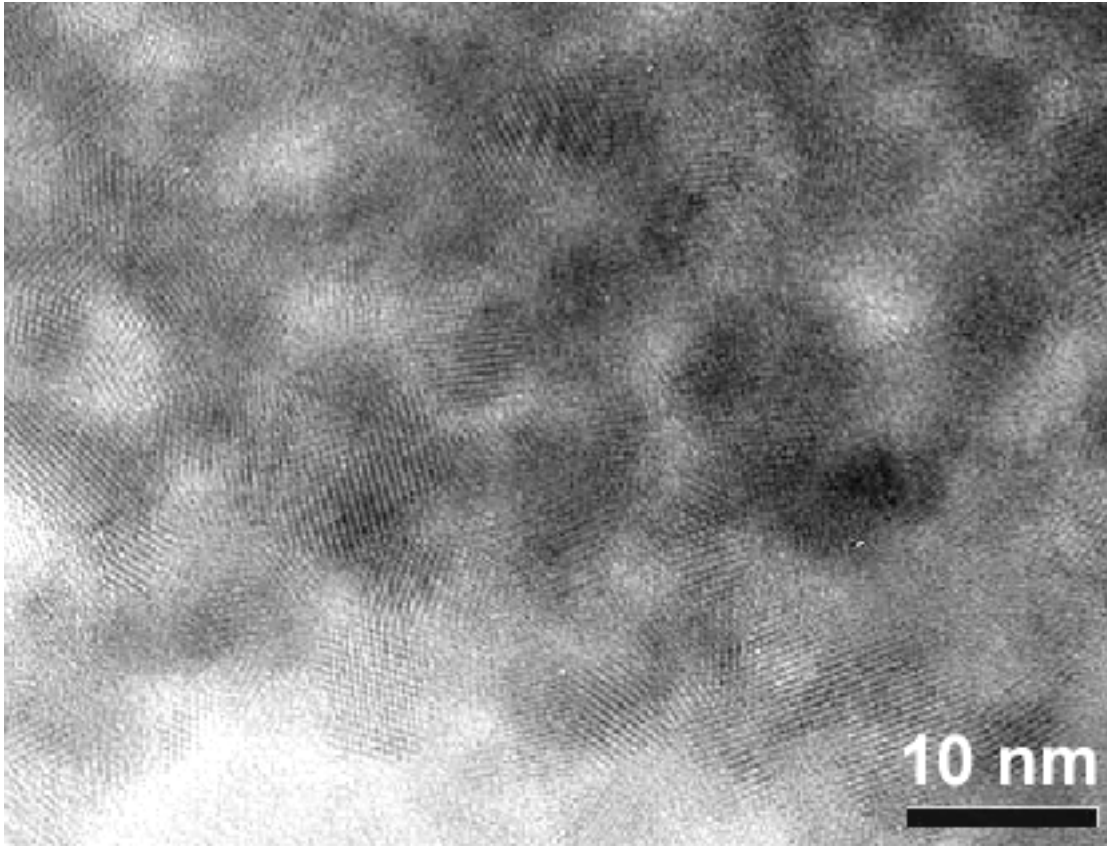


Figure 11. TEM Micrograph of 65.2 at. % Zr after 106 hr of Heat Treatment at 700 °C

As the deposition continues the electrode surface is covered with powder and an ohmic drop is incorporated into the value of applied potential. The ohmic contribution was confirmed by impedance spectroscopy and values of the increasing resistance between the reference and cathode is provided in Table 2. The actual potential, then at the working electrode is given by elimination of the ohmic potential drop, $E = E_{app} - IR$.

Figure 14 shows the current-potential relationship with the ohmic component removed. The current decreases at a given potential with deposition time and is indicative of the rate of generation of OH^- necessary for co-precipitation of ceria-zirconia.

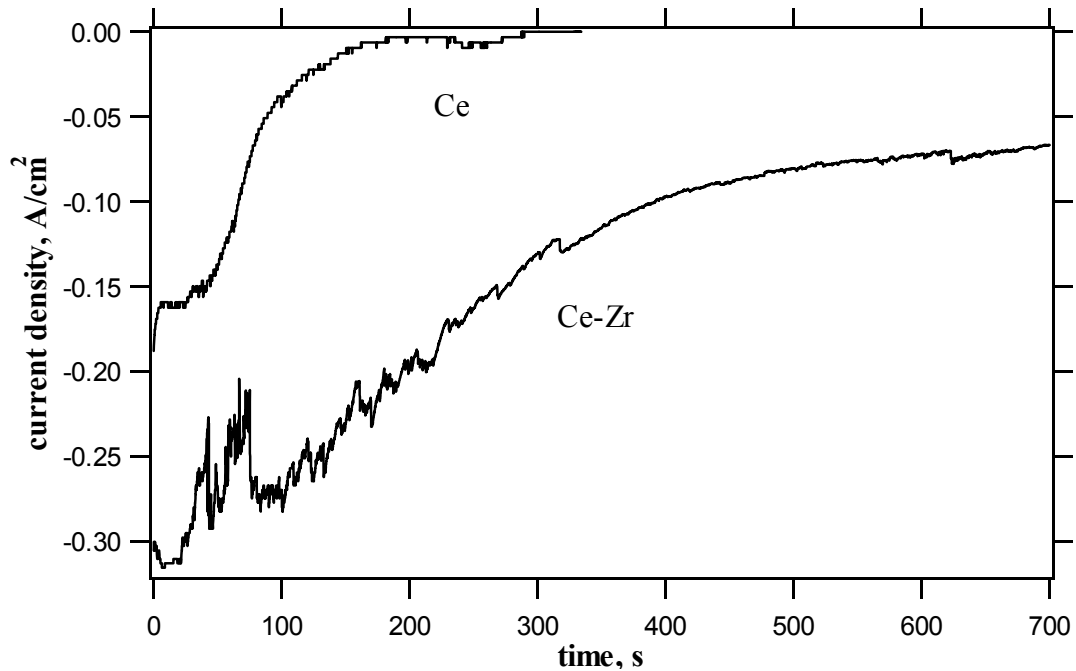


Figure 12. Current Characteristics for the Ce and Ce-Zr Electrolyte at an Applied Potential of -2.0 V and Stagnant Solution.

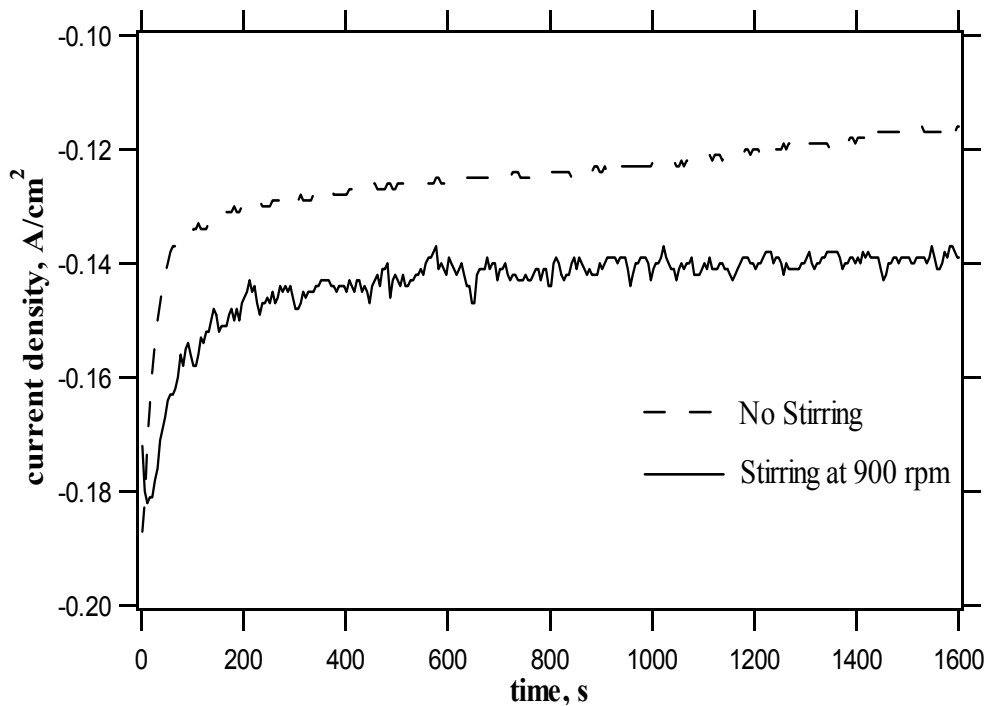


Figure 13. Current Characteristics of Ceria-Zirconia in Quiescent Solution and With a Stirring Speed of 900 rpm, Both With an Applied Potential of -2.0 V.

Table 2. Resistivity of solution C at various times of deposition.

Resistivity, R, ohms	Time of Deposition, mins
5.41	0
7.82	30
24.13	60
34.76	90

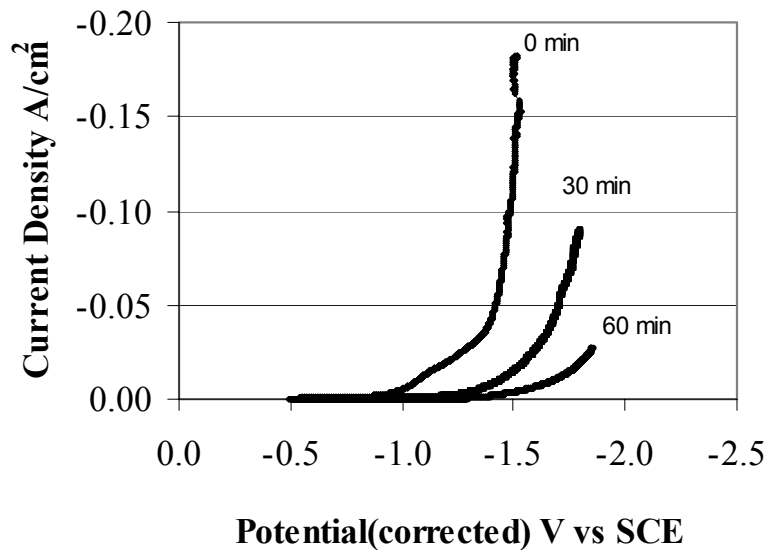


Figure 14. Polarization Curves Corrected for Ohmic Drop, Solution C for a Scan Rate of 5 mv/s.

3. HIGH TEMPERATURE DESULFURIZATION

3.1. Fixed-Bed Reactor

Sorbent performance during H₂S removal is evaluated using the fixed-bed reactor system shown in Figure 15. Gases – H₂S, H₂, N₂, and CO₂ – are obtained from high purity cylinders and flow rates are controlled using calibrated mass flow controllers. The proportions of H₂ and CO₂ in the feed gas can be adjusted to control the reducing power (oxygen partial pressure) of the feed gas. Valves are arranged so that either feed or product gas can be fed to the gas chromatograph for analysis. In addition, N₂ feed gas can be directed past a calibrated H₂S permeation tube where a standard quantity of H₂S is added for calibration of the gas chromatograph at low H₂S concentrations (< 10 ppmv). Calibration at higher H₂S concentrations is accomplished by mixing pure cylinder gases using the mass flow controllers.

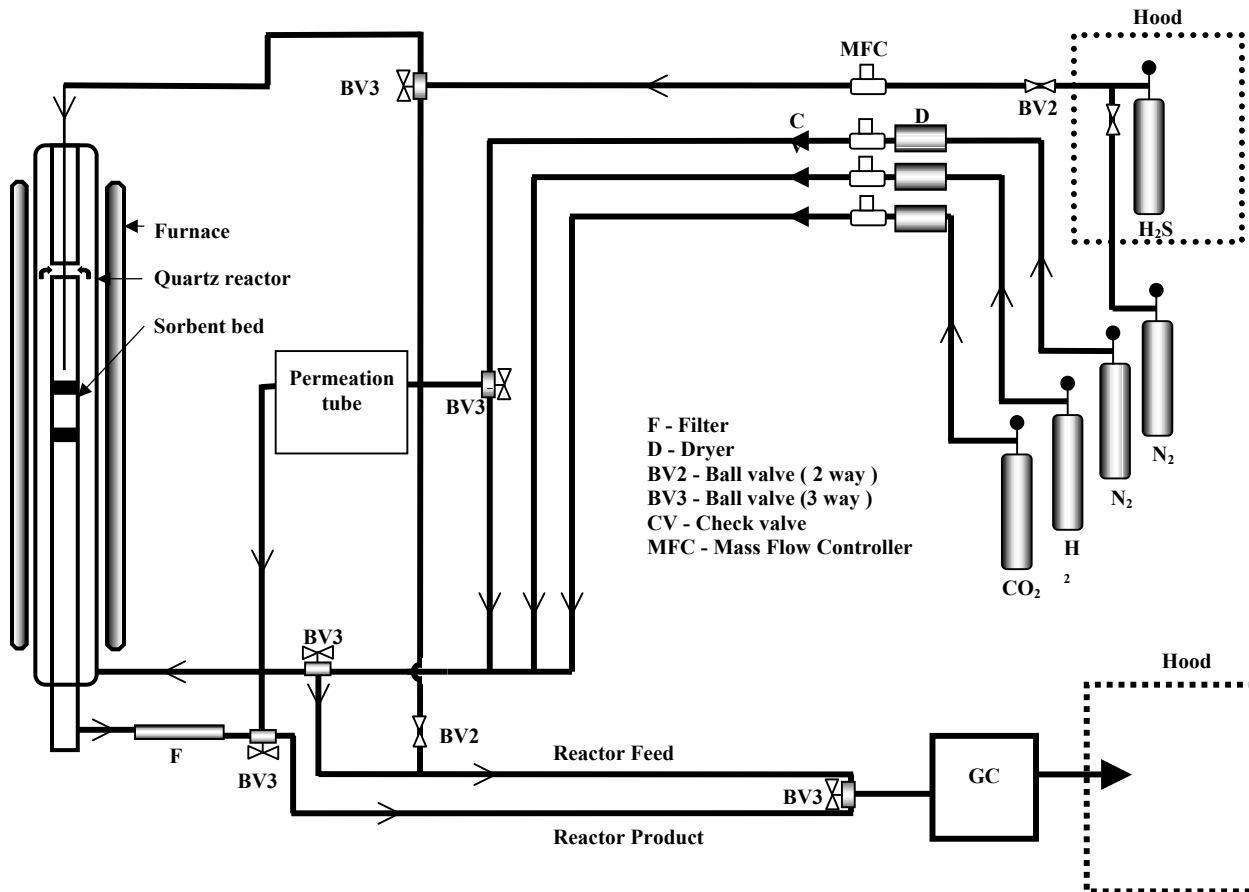


Figure 15. Fixed-Bed Reactor System

In normal operation H_2 , CO_2 , and N_2 are mixed in the desired proportions and fed to the bottom of the quartz reaction vessel. These gases are preheated as they flow upward in the annular region outside of the reactor insert. H_2S is added to the preheated gases just before they contact the sorbent bed, which is supported inside the reactor on a porous quartz disc and quartz wool. Sorbent pre-reduction, if used, is carried out in the same manner except that H_2S is not added. Product gas exits from the bottom of the reactor, and flows through a quartz wool filter to remove any particulate matter and/or traces of elemental sulfur that may be present, and to the gas chromatograph for analysis.

All components except the pure gas feed lines, including the reactor vessel and insert, and all valves, are of quartz or teflon to prevent interaction between low concentrations of H_2S and steel surfaces. Steel surfaces within the gas chromatograph are silco-treated to eliminate interaction.

A more detailed diagram of the reactor, including dimensions, is shown in Figure 16. The total capacity of the reactor is approximately 15 g of solid.

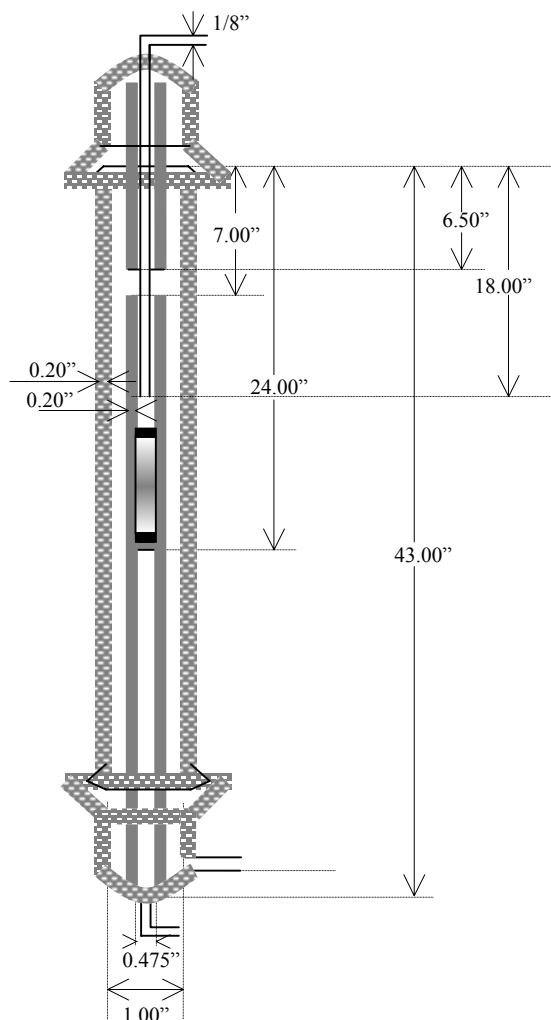


Figure 16. Details of the Quartz Reactor

3.2. Gas Analysis

H₂S concentration of the feed and product gas is determined using a Varian model 3800 gas chromatograph purchased for this project using LSU matching funds. The chromatograph is equipped with dual columns, two Valco multiport sampling valves, and both a pulsed flame photometric detector (PFPD) and a thermal conductivity detector (TCD). The PFPD is used for H₂S concentrations from sub-ppmv to about 10 ppmv, while the TCD is used for concentrations in excess of 100 ppmv. There is a gap in the analytical capability between about 10 and 100 ppmv, but primary interest is in the low concentration range. The PFPD provides analytical capability to approximately 0.1 ppmv H₂S (100 ppbv) and is about 10 times more sensitive than a standard flame photometric detector.

A summary of chromatograph operating conditions is presented in Table 3.

Table 3. Gas Chromatograph Operating Conditions

PFPD	Column:	CP SIL5, 5 μ L = 3 m, D = 530 μ , T = 200°C
	Carrier Gas:	He, 2.9 ml/min
	Sample Loop:	SilcoSteel, 50 μ L
TCD	Column:	HAYESEP A SilcoSteel L = 3.3 m, D = 3.13 μ , T = 200°C
	Carrier Gas:	He, 28 ml/min He, 31.2 ml/min (backflush)
	Sample Loop:	SilcoSteel, 2 ml

The flow arrangement through the two automatic valves (one 10-port and one 6-port) is shown in Figure 17. In normal operation shown in the upper left diagram the gas to be analyzed enters the 10-port valve at position 4, exits to the PFPD sample loop at position 5, re-enters the 10-port valve at position 8, exits to the TCD sample loop at position 9, again enters the 10-port valve at position 2 and is vented to a laboratory hood through position 3. In this operation mode the contents of both sample loops are continually purged and replenished with the most recent product gas. Three carrier gases are used. Carrier 1 enters the 10-port valve at position 7 and exits at position 6 to the PFPD column and then to the PFPD. Carrier 2 enters the 10-port valve at position 10, exits at position 1, and flows to the 6-port valve. It enters the 6-port valve at position 2 and exits through position 1 to the TCD column, then back into the 6-port valve at position 3 and out through position 4 to the TCD and laboratory vent. Carrier 3 enters the 6-port valve at position 5 and exits through position 6 to vent.

Samples for both the PFPD and TCD are acquired simultaneously by switching the 10-port valve to the position shown in the upper right diagram of Figure 17. The gas sample enters the 10-port valve at position 4 and exits through position 3 directly to the laboratory vent. Carrier gas 1 enters the 10-port valve at position 7, exits through position 8 and picks up the sample from the PFPD sample loop. It reenters the 10-port valve at position 5 and exits through position 6 to the PFPD column. Column effluent then flows directly to the PFPD. Carrier gas 2 enters at position 10 and exits through position 9 where it picks up the TCD sample. It re-enters the 10-port valve at position 2 and exits through position 1 to the 6-port valve. The TCD sample enters the 6-port valve at position 2 and exits to the TCD column through position 1. The TCD column effluent re-enters the 6-port valve at position 3 and exits through position 4 to the TCD. Flow of carrier 3 is unchanged. It enters the 6-port valve at position 5 and exits through position 6 to vent.

The position of the 6-port valve is switched in the lower center diagram of Figure 17 to permit H₂O formed during the desulfurization reaction to be backflushed to vent. Switching occurs after H₂S has been eluted from the TCD column but before water is eluted. Sample gas and carrier gas 1 flows are not changed from the previous case. However, with the 6-port valve in the new position, carrier gas 2 flows through the 10-

port valve as before. It enters the 6-port valve at position 2, exits through position 3, and flows in the reverse direction through the TCD column to backflush the H₂O. Carrier gas 2 plus the H₂O then re-enters the 6-port valve at position 1 and exit through position 6 directly to vent. Carrier gas 3 enters the 6-port valve at position 5 and exits through position 4 to the TCD so that carrier gas flow is maintained through the TCD at all time.

PFPD calibration was accomplished by flowing N₂ at a known rate past a calibrated H₂S permeation tube maintained at 30°C (see Figure 15). A PFPD calibration curve between 0.1 and 6 ppmv H₂S is shown in Figure 18. The chromatogram obtained from the 0.1 ppmv sample shown in Figure 19 indicates that the signal-to-noise ratio is strong even at this low H₂S concentration. The best calibration was obtained by correlating H₂S peak height versus H₂S concentration using a third order polynomial with a zero intercept. The calibration equation shown on the figure has a R² value of 0.9982.

TCD calibration was accomplished by mixing N₂ and H₂S from the high purity cylinders with flow rates controlled using the mass flow controllers. Results of the TCD calibration between 100 ppmv and 1.5% (15,000 ppmv) are shown in Figure 20. The calibration was also based on H₂S peak height using a second order polynomial with a zero intercept and the R² value was 0.9996.

3.3. Materials

Preliminary tests using two sorbents have been completed at this point. The first, pure CeO₂ from Rhone Poulenc, is the same material used in the earlier studies (Zeng et al. 1999 and Zeng et al. 2000). In addition, a commercially available CeO₂-ZrO₂ material from NexTech Materials, Ltd., containing 80 mol% CeO₂ and 20 mol% ZrO₂ has been tested. Selected properties of these materials, as provided by the supplier, are presented in Table 4.

Table 4. Selected Properties of CeO₂ and CeO₂-ZrO₂ Used in Preliminary Fixed-Bed Reactor Tests

	Rhone Poulenc CeO ₂	NexTech CeO ₂ -ZrO ₂
Composition	91 wt % CeO ₂ 9 wt% volatiles	80 mol% CeO ₂ 20 mol% ZrO ₂
Particle Size*	150-300 μm	150-300 μm
Surface Area	156 m ² /g **	64 m ² /g ***

- * after tableting, crushing, and sieving
- ** reported by Zeng (1999a)
- *** reported by NexTech

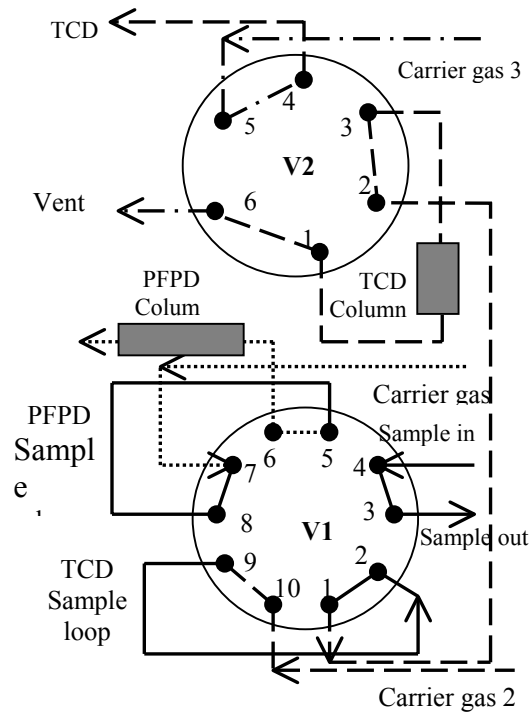
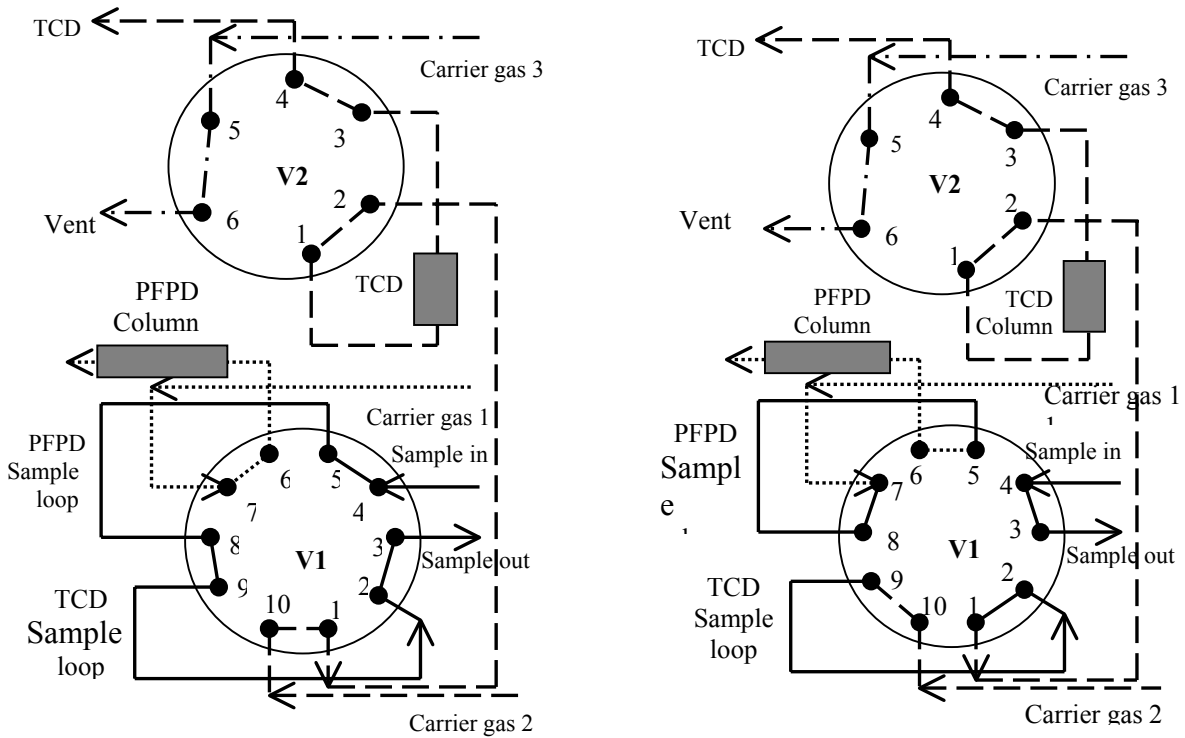


Figure 17. Chromatograph Sampling Arrangement

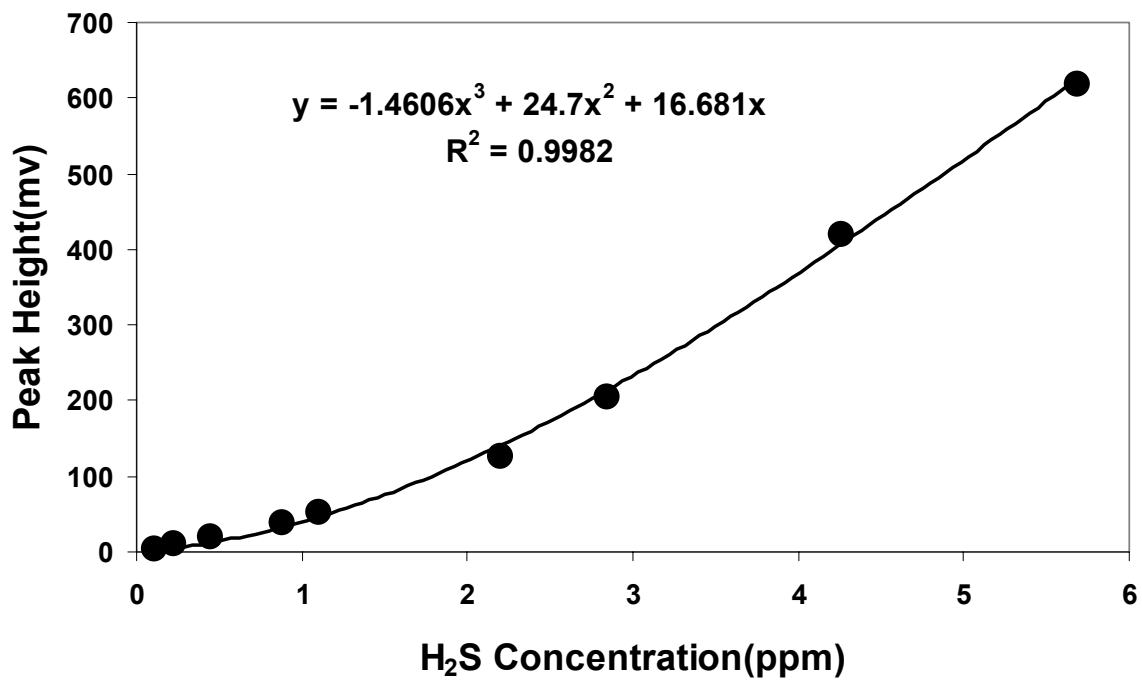


Figure 18. PFPD Calibration Curve

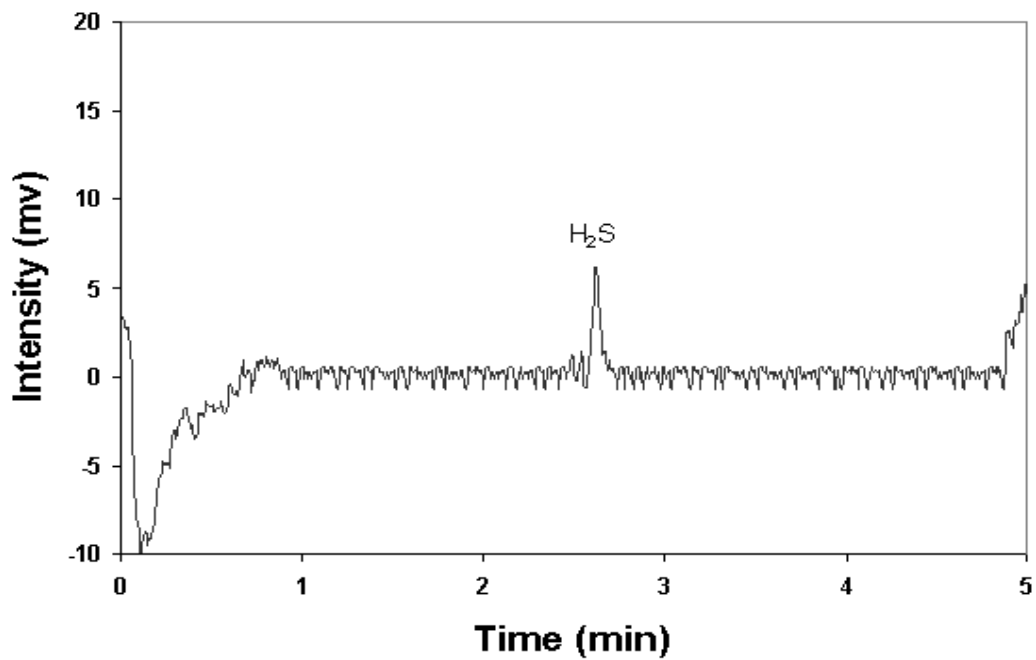


Figure 19. PFPD Chromatogram at 0.01 ppmv H₂S

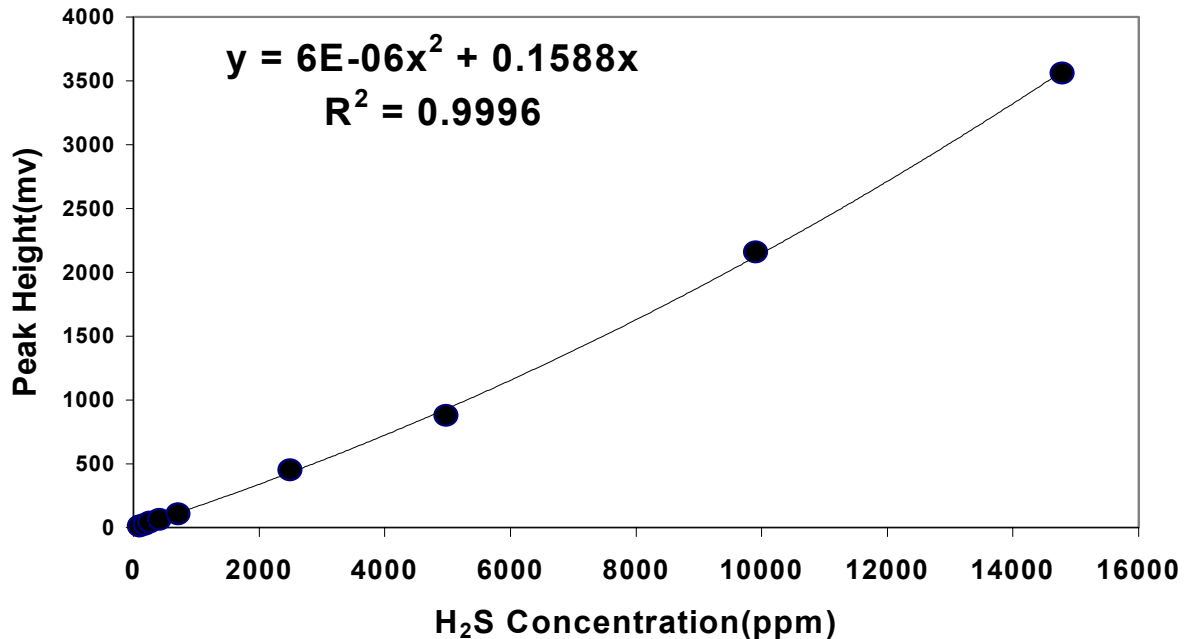


Figure 20. TCD Calibration Curve

The sorbent, either CeO₂ or CeO₂-ZrO₂, was first pressed into tablets using a hydraulic press at 20,000 psi. The resulting tablets were then crushed and sieved with the 150-300 μm size range used in reaction tests. Sorbent was then mixed with Al₂O₃ in a 2-to-1 ratio by weight and a selected amount of the mixture was added to the reactor. Tablets were formed because the small particle size of the as-received sorbent materials produced excessive pressure drop through the reactor, and the Al₂O₃ was added to control sintering. Zeng et al. (1999) found that the sorbent without Al₂O₃ sintered into a loosely bound chalk-like mass after testing. With the added Al₂O₃ the mixture could be removed from the reactor as a free-flowing powder after tests.

3.4. Preliminary Results

Only a limited number of preliminary tests were completed during the first year of the project. A typical breakthrough curve showing H₂S concentration as a function of dimensionless time is shown in Figure 21.

During the early stages of the reaction H₂S removal is almost complete and, on this scale, the H₂S concentrations appears to be zero. Breakthrough begins at a dimensionless time, t^* , about 0.5, and the H₂S concentration gradually increases and approaches the inlet concentration at $t^* \approx 1.8$. Dimensionless time is defined as the ratio of the actual reaction time to the time t^* corresponding to complete conversion of CeO₂ if

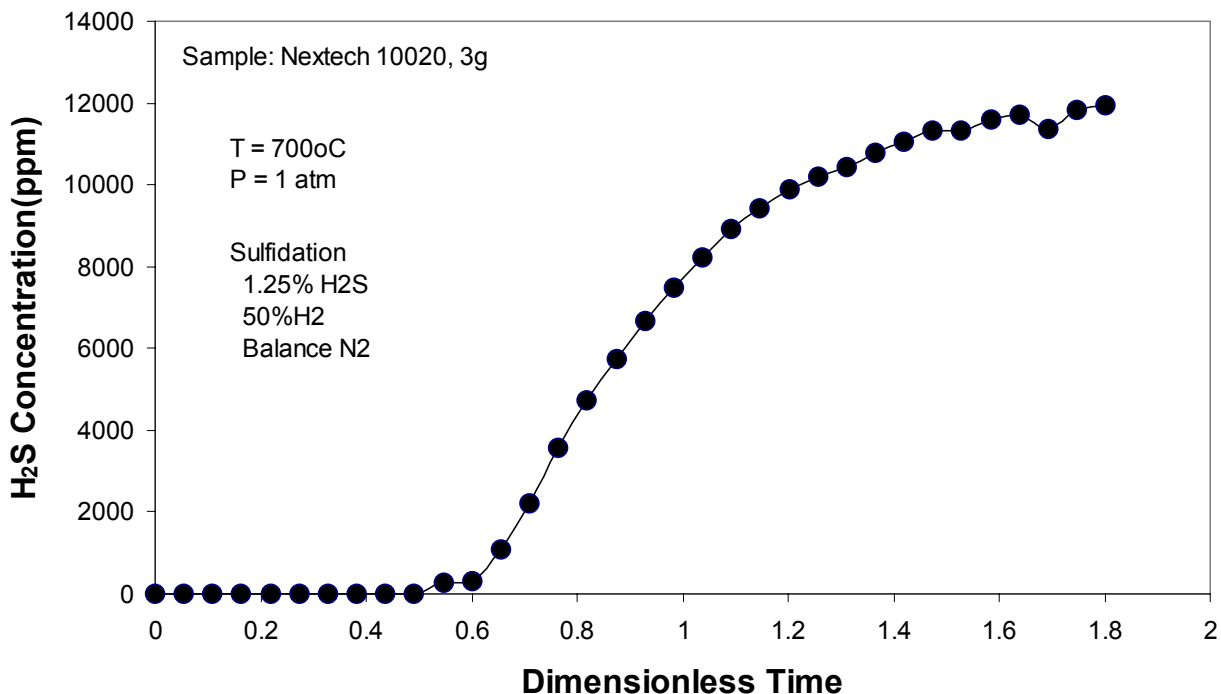


Figure 21. Typical Breakthrough Curve Showing H₂S Concentration in the Reactor Product as a Function of Time.

100% of the H₂S fed were removed, and for practical purposes is almost equal to the fractional conversion of CeO_n to Ce₂O₂S.

Our primary interest is on the low H₂S concentrations obtained during the initial periods of the test and the following figures show only the early portions of the breakthrough curve. Zeng et al. (2000) found that pre-reduction of the CeO₂ sorbent in an H₂S-free atmosphere would provide increased H₂S removal efficiency compared to direct sulfidation in a reducing atmosphere. This result is confirmed in Figure 22 where H₂S concentration in the product gas is plotted versus dimensionless time, t*.

Rhone Poulenc CeO₂ was used in these tests, and reaction conditions are noted on the figure. Without pre-reduction the H₂S concentration was about 4 ppmv for 0.1 < t* < 0.3, increased to about 8 ppmv for 0.35 < t* < 0.45, and then increased to levels beyond the range of the PFPD in the next sample. With pre-reduction the H₂S concentration was equal to or less than 1 ppmv for t* < 0.3 and then exceeded the PFPD limit at t* ≈ 0.4.

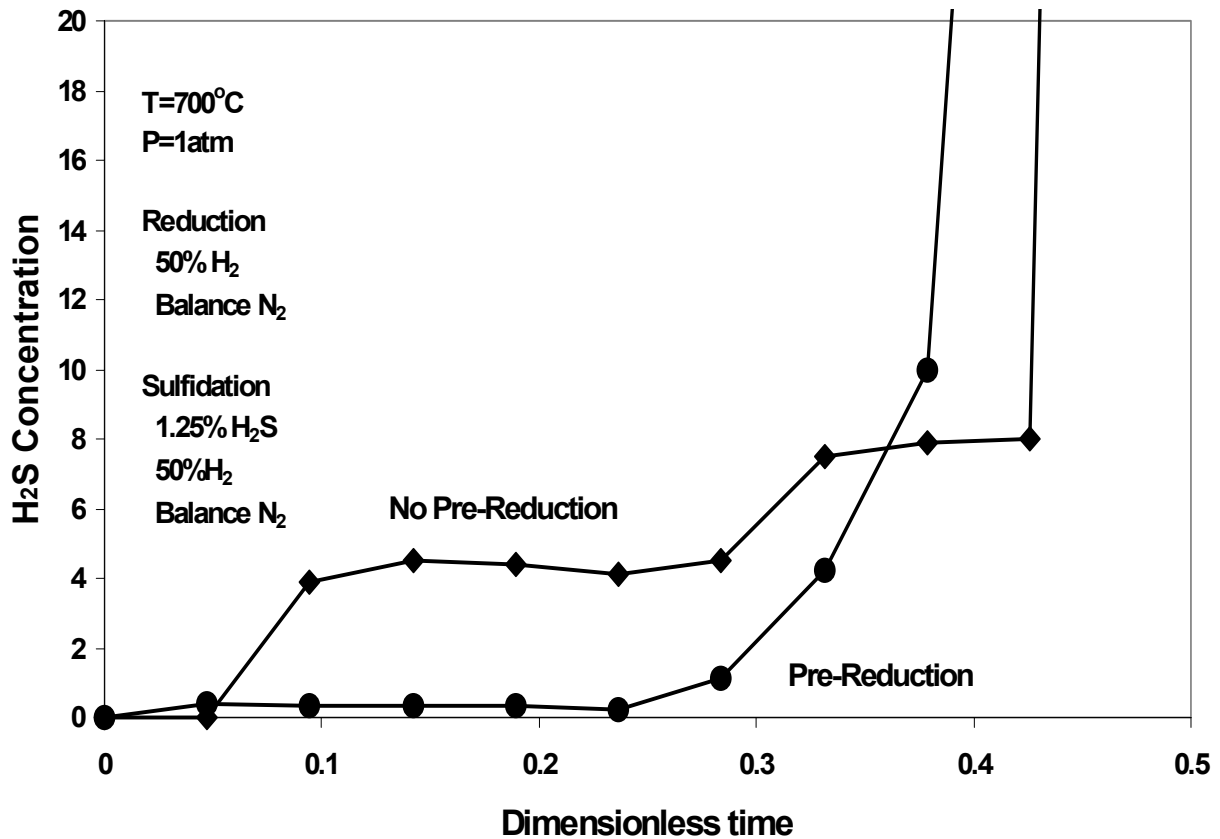


Figure 22. The Effect of Pre-Reduction on H₂S Concentration Using CeO₂ Sorbent.

Figure 23 compares the results of tests using pre-reduced CeO₂ and pre-reduced CeO₂-ZrO₂ at the same reaction conditions. The H₂S concentration was less than 1 ppmv with both sorbents during the early phases of the test. However, the H₂S concentration in contact with CeO₂-ZrO₂ sorbent was near the 0.1 ppmv detection limited of the PFPD for $t^* < 0.3$, while the H₂S concentration was about 0.3 ppmv in contact with CeO₂ for the same dimensionless time period.

While these preliminary tests used much stronger reducing gases than associated with typical coal derived gases, the results are favorable. The advantages associated with pre-reduction have been confirmed and it appears that the addition of ZrO₂ to CeO₂ produces the type of results that are hoped for.

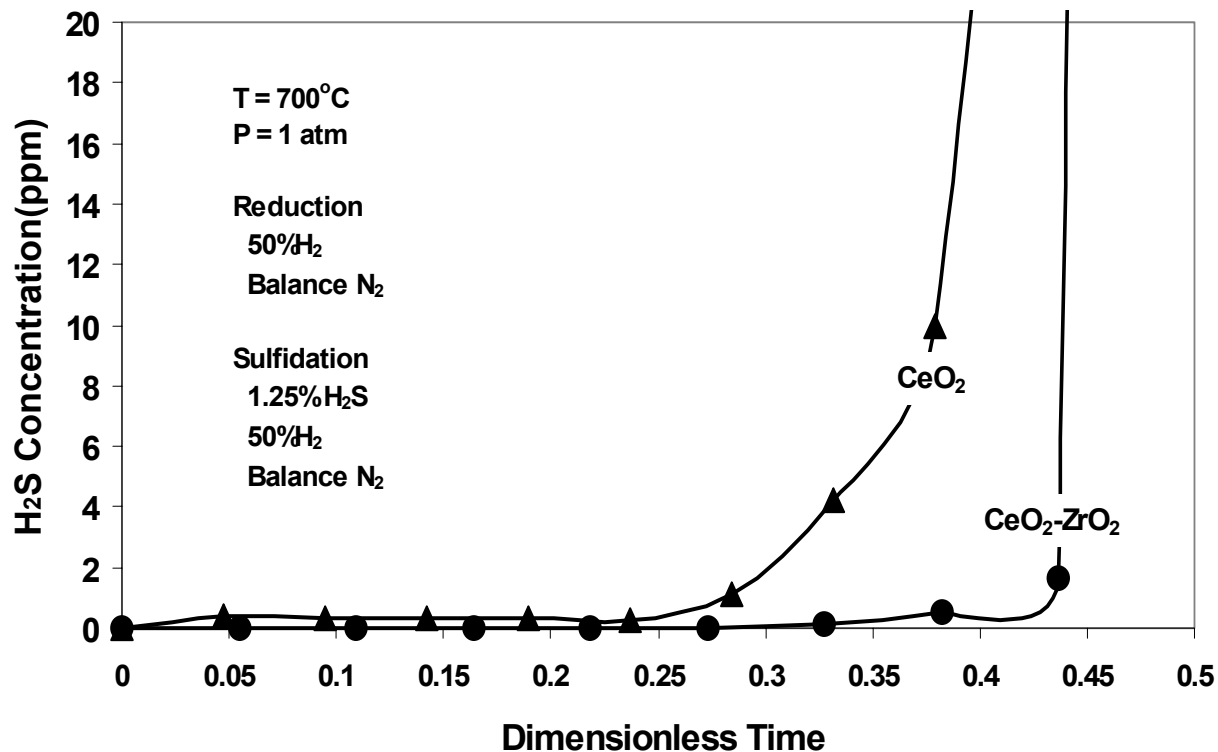


Figure 23. Comparison of H₂S Concentrations Using CeO₂-ZrO₂ and CeO₂.

4.0. CONCLUSIONS

The electrochemical method of producing CeO₂-ZrO₂ powders with nanometric crystallites and a varied composition range was demonstrated. To our knowledge, this is the first successful electrosynthesis of CeO₂-ZrO₂ powders. Comparison of the electrosynthesized powder to a commercial one with similar composition confirmed the same XRD pattern of a single, solid solution phase, with finer crystallite size. The electrosynthesized powder has not yet been tested for H₂S removal.

It is currently premature to make definite conclusions concerning the ability of CeO₂-ZrO₂ sorbents to satisfy the DOE Vision 21 desulfurization goal since only a very limited number of preliminary tests have been completed. The preliminary results, however, are encouraging. The level of H₂S removal is increased when both test sorbents, pure CeO₂ and CeO₂-ZrO₂, are pre-reduced in a sulfur-free reducing gas prior to sulfidation compared to simultaneous reduction-sulfidation. In addition, pre-reduced CeO₂-ZrO₂ appears to be more effective than pure CeO₂ in removing H₂S. The prebreakthrough H₂S concentrations in tests at 700°C and 1 atm using a feed gas containing 1.25% H₂S, 50% H₂, balance N₂ were at the lower PFPD calibration limit of

0.1 ppmv (100 ppbv) using pre-reduced CeO₂-ZrO₂ compared to about 0.3 ppmv (300 ppbv) using pre-reduced CeO₂.

5.0. REFERENCES

- Bevan, D. and Kordis, J., 1964, Mixed Oxides of the Type MoO₃ – 1. Oxygen Dissociation Pressure and Phase Relationship in the System CeO₂-Ce₂O₃ at High Temperatures, *Journal of Inorganic and Nuclear Chemistry*, 26, 1509.
- Bunluesin, T., Gorte, R., and Graham, G., 1997, CO Oxidation for the Characterization of Reproducibility in Oxygen Storage Components of Three-Way Automotive Catalysts, *Applied Catalysis B., Environmental*, 14, 105.
- Colon, G., Pijolat, M., Valdivieso, F., Vidal, H., Kaspar, J., Daturi, M., Binet, C., Lavalley, J., Baker, R., and Bernal, S., 1998, Surface and Structural Characterization of Ce_xZr_{1-x}O₂ Mixed Oxides as Potential Three-Way Catalyst Promoters, *Journal of the Chemical Society, Faraday Transactions*, 94, 3717.
- Cuif, J.-P., Blanchard, G., Touret, O., Marczi, M., and Quemere, E., 1996, Proceedings of the 1996 International Fall Fuels and Lubricants Meeting of the Society of Automotive Engineers, San Antonio, TX, 73.
- Focht, G. D., Ranade, P. V., and Harrison, D. P., 1988, High Temperature Desulfurization Using Zinc Ferrite: Reduction and Sulfidation Kinetics, *Chemical Engineering Science*, 43, 3005.
- Gibson, J. B., and Harrison, D. P., 1980, The Reaction Between Hydrogen Sulfide and Single Spherical Pellets of Zinc Oxide, *Industrial and Engineering Chemistry, Process Design and Development*, 19, 231.
- Harrison, D. P., 1998, Performance Analysis of ZnO-Based Sorbents in Removal of H₂S from Fuel Gas, in *Desulfurization of Hot Coal gas*, A. Atimtay and D. P. Harrison, eds., Springer, Berlin, 213.
- Hori, C., Permana, H., Ng, K., Brenner, A., Moore, K., Rahmoeller, K., and Belton, D., 1998, Thermal Stability of Oxygen Storage Properties in a Mixed CeO₂-ZrO₂ System, *Applied Catalysis B, Environmental*, 16, 105.
- Ozawa, M., 1997, Role of Cerium-Zirconium Mixed Oxides as Catalysts for Car Pollution: A Short Review, *Journal of Alloys and Compounds*, 275, 886.
- Podlaha, E.P., Bogli, A., Bonhote, Ch. and Landolt, 1997, Development of a New, Pseudo-Inverted Disk Electrode, *D. Journal of Applied Electrochemistry*, 27, 805.

- Sorensen, O., 1976, Thermodynamic Studies of the Phase Relationships of Nonstoichiometric Cerium Oxides at Higher Temperatures, *Journal of Solid State Chemistry*, 18, 217.
- Switzer, A., 1987, Electrochemical Synthesis of Ceramic Films and Powders, *Journal of the American Ceramic Society Bulletin* , 66[10], 1521.
- Trovarelli, A., 1996, Catalytic Properties of Ceria and CeO₂-Containing Materials, *Catalysis Reviews: Science and Engineering*, 38, 439.
- Trovarelli, A., de Leitenburg, C., and Colcetti, G., 1997, Design Better Cerium-Based Oxidation Catalysts, *CHEMTECH*, 27, 32.
- Woods, M. C., Gangwal, S. K., Jothimurugesan, K., and Harrison, D. P., 1990, The Reaction Between H₂S and Zinc Oxide-Titanium Oxide Sorbent: 1. Single Pellet Kinetic Studies, *Industrial and Engineering Chemistry Research*, 29, 1160.
- Zamar, F., Travarelli, A., de Leitenburg, C., and Dolcetti, G., 1995, CeO₂-Based Solid Solutions with the Fluorite Structure as Novel and Effective Catalysts for Methane Combustion, *Journal of the Chemical Society, Chemical Communications*, 965.
- Zeng, Y, Zhang, S., Groves, F. R., and Harrison, D. P., 1999, High Temperature Gas Desulfurization with Elemental Sulfur Production, *Chemical Engineering Science*, 54, 3007.
- Zeng, Y., 1999a, Cerium Oxide as a Highly Effective and Durable High Temperature Desulfurization Sorbent, Ph. D. Dissertation, Louisiana State University.
- Zeng, Y., Kaytakoglu, S., and Harrison, D. P., 2000, Reduced Cerium Oxide as an Efficient and Durable High Temperature Desulfurization Sorbent, *Chemical Engineering Science*, 55, 4893.
- Zhou, Y. Phillips, R.J. and J. Switzer, 1995, Electrochemical Synthesis and Sintering of Nanocrystalline Cerium(IV) Oxide Powders, *Journal of the American Ceramic Society*, 78, 981-85.